

112 pages

On The Extension of the MCSCF/CI Method

Final Report Covering Period September 15, 1981  
through August 31, 1984

Supported under NASA Cooperative Agreement NCC2-158

NASA Technical Officer:

Dr. David Cooper

NASA Ames Research Center  
STC: 230-3  
Moffett Field, CA 94035

Principal Investigators:

Dr. Charles Bauschlicher Jr.

Dr. Constance J. Nelin

Dr. Andrew Komornicki

Polyatomics Research Institute  
1101 San Antonio Rd. Suite 420  
Mountain View, CA 94043

(NASA-CR-176933) ON THE EXTENSION OF THE  
MCSCF/CI METHOD Final Report, 15 Sep. 1981  
- 31 Aug. 1984 (Polyatomics Research, Inc.)  
112 p

CSSL 07D

N86-29924  
THRU  
N86-29929  
Unclas  
43495

G3/25

TABLE OF CONTENTS

---

INTRODUCTION .....	1
FINAL REPORT OF C.W. Bauschlicher.....	
FINAL REPORT OF C.J. Nelin .....	
FINAL REPORT OF A. Komornicki .....	

# INTRODUCTION:

The enclosed document is the final technical report on the work performed under NASA Cooperative agreement NCC2-158.

This work covers the reports of three principal investigators who contributed to this work during the tenure of this project.

This this report is a composite of three reports of:

Dr. C.W. Bauschlicher, Dr. C.J. Nelin, and Dr. A. Komornicki

The work where Dr. Komornicki was principal investigator was carried out by Dr. J. Almlof, of Oslo Norway.

The following is the final report of Dr. C.W. Bauschlicher Jr. who was the principal investigator on this grant from September 15, 1981 through June 30, 1982, at which point he resigned his position with the Institute.

This report provided interim status on this grant, and was submitted to NASA technical personnel in January 1983.

YEAR END REPORT ON COOPERATIVE AGREEMENT NCC2-158

Prepared by:


POLYATOMICS RESEARCH INSTITUTE  
1101 San Antonio Road, Suite 420  
Mountain View, CA 94043

Submitted to:

NASA Ames Research Center  
Moffett Field, CA 94035

Date:

January 11, 1983



---

Andrew Komornicki  
Director

## Introduction

Recent research has focused on two main areas, 1) bonding in transition metal oxides and 2) adsorption of CO and Al and Ni. In both of these theoretical studies a major interest was to obtain a better understanding of the nature of the bonding in transition metal containing systems. These calculations while useful themselves for the systems studied can also serve as a calibration of the methods employed when they are later applied to larger systems. These ab initio studies used self consistent field (SCF), multi-configuration self consistent field (MCSCF) and configuration interaction (CI) methods in the treatment of the transition metal oxides and only the SCF method for the adsorption studies. In order to obtain reliable results, basis sets of reasonable quality were used. The contracted Gaussian basis sets used were of double zeta quality or better in the core and valence region or in the case of Al in the valence region alone (the core having been contracted to single zeta using a segmented contraction). Further to be able to treat larger systems, for Ni the modified effective core potential (MEP) of Goddard (with the "4p" functions of Melius) was employed for the neighboring Ni atoms to the adsorption site and for the Al neighbors used 3 electron ECP's. These studies have been carried out in collaboration with Paul S. Bagus (IBM, San Jose) and Charles W. Bauschlicher (Ames).

The transition metal oxide calculations focused on the two systems: CrO and MoO. These were part of a larger study (with Paul Bagus and Charles Bauschlicher) which also included NiO, PdO, CuO and AgO. Through this study both the effects of moving across the row (varying the number of d electrons) as well as moving down a column could be observed. In CuO there was no obvious direct involvement of the d electrons in the bond, in NiO there were excited states which had direct d involvement in the bond, whereas in CrO the lowest states formed Crd - Op bonds. These systems are primarily (Metal)<sup>+</sup> (O)<sup>-</sup> with a charge of ~0.7 electrons. For Cr<sup>+</sup> the experimental d<sup>5</sup> (ground state) - d<sup>4</sup>s<sup>1</sup> separation is ~12,000cm<sup>-1</sup> (SCF ~9,200cm<sup>-1</sup>). Considering this large separation, it is surprising and still unresolved why many of the CrO states have as much d<sup>4</sup> character as

as they do. Often the states have d populations (near equilibrium) of approximately 4.3. For MoO the d populations for the high spin states are approximately 4.6. (The experimental  $d^5-d^4s^1$  separation for  $Mo^+$  is  $\sim 12,500cm^{-1}$ ; the SCF value is  $\sim 18,000cm^{-1}$ .) At this point the changes between first and second row appear to be small, however the work on MoO is still quite incomplete as only high spin states have been calculated thus far. Unlike the dimers  $Cr_2$  and  $Mo_2$  where Goodgame and Goddard found only an s-s bond for  $Cr_2$  but a bond involving d for  $Mo_2$ , CrO has clear d involvement in the bond. There are however larger s populations in many of the CrO states, especially the high spin states, than in MoO.

One other striking feature of the CrO calculation is the radical bond shortening which occurs when configurations involving excitations from  $O2p\pi$  are included. At the MCSCF level the bond shortening was  $0.1\overset{\circ}{A}$  and at the CI level it was  $\sim 0.2\overset{\circ}{A}$ . These configurations also contributed to bond shortening in NiO and CuO, though it was a much smaller effect in these systems.

In the CO adsorption studies Al and Ni were chosen as substrates so the effects of the valence sp electrons could be studied first alone (Al) and then in the presence of d electrons. A possible bonding mechanism involving mainly the valence electrons was first observed in a study of NiCO. It was seen that a state which had a valence configuration of  $4sp\sigma^1$  was very weakly bound whereas a state which had  $4p\pi^1$  was much more strongly bound. It was postulated that an increased  $p\pi$  population increased bonding with  $CO(2\pi^*)$  whereas an increased  $sp\sigma$  population increased repulsion due to overlap with the CO  $5\sigma$ .

When clusters ranging in size from 1 metal atom to 9 metal atoms were calculated there was a changing balance between these two competing effects. With no neighbors (AlCO, NiCO) the state was either  $sp\sigma^1$  or  $p\pi^1$  and unbound or bound (or barely unbound) accordingly. In the larger clusters the shape of the cluster tended to strongly affect the valence balance, i.e. lower layers reduced repulsion by "getting the  $\sigma$  electrons out of the way", whereas neighbors on the same layer would compete for the electrons hence reducing the bonding. In all cases it appeared

that the outer atoms donated charge to the central atom and bonding was dependent upon whether the  $\sigma$  or  $\pi$  population increased. Although the role of the d electrons in the Ni clusters was never totally clear, when the clusters were treated as all 1 electron Ni atoms (the d's now part of the MEP) there was no longer any CO backbonding, thus the d electrons appear to certainly be involved in some subtle way.

On the basis of the valence population arguments it can be predicted that the order of binding with CO would be greatest for Na then decreasing for Mg and Al, i.e. the system with a smaller s population would be favored. Also transition metals would be favored as they have in general  $\leq 1$  valence sp electron.

In the next two sections some detail on the oxide and adsorption calculation will be presented.



## Transition Metal Oxides: CrO and MoO

The transition metal oxides are being studied because of their use as a basis for later treatments of chemisorption and oxidations of metal surfaces. Models for these processes will be substantially more involved than a "simple" diatomic. However the methods used must be calibrated for the diatomics and the features of the diatomic bonding must be understood before substantial surface related work can be undertaken.

The contracted Gaussian orbital basis set for Cr is that of Wachters including two function to represent the 4p orbital and also including Hay's diffuse d function (14s11p6d/8s6p4d). The oxygen basis set is based on Dunning's double zeta contraction of Huzinaga's set, including also a diffuse p,  $\alpha = 0.059$  to represent the  $O^-$  character and a d  $\alpha = 0.90$  (9s6p1d/4s3p1d). The Mo basis set is Huzinaga's set contracted using a generalized contraction (17s13p9d/7s7p4d).

For both Cr and Mo the ground states are  $^7S(d^5s^1)$  and the first excited states are  $^5D(d^4s^2)$ . For  $Cr^+$  and  $Mo^+$  the ground states are  $^6S(d^5)$  and the first excited states are  $^6D(d^4s^1)$ . Both CrO and MoO are highly ionic molecules which are basically  $Metal^+$  and  $O^-$  in character. For  $O^-$  in  $C_{\infty v}$  symmetry there are two possible states:  $\sigma^1\pi^4$  ( $\sigma$  hole) and  $\sigma^2\pi^3$  ( $\pi$  hole). When  $O^-$  is combined with either  $Cr^+$  or  $Mo^+$ , both  $^5,7\Sigma^+$  and  $^5,7\Pi$  states can be formed. (The  $^5\Pi$  is the experimentally observed ground state). For both systems these four states are being calculated, with the  $^7\Sigma^+$  and  $^7\Pi$  states being treated at the SCF and CI levels, and the  $^5\Sigma^+$  and  $^5\Pi$  states being treated at the MCSCF and CI levels. The work on both systems is still ongoing.

For the lower spin states two types of MCSCF calculations are considered. These are characterized by the configurations for which the orbitals are optimized. In the small calculation on the  $^5\Sigma^+$  states 6 electrons are distributed among the 5  $Cr^+3d$  orbitals and the  $O^-2p\sigma$  orbital. In the large calculations there are 10 electrons and the  $O^-2p\pi$  orbitals are also included. The CI performed was all singles and doubles from the

six important configurations in the small MCSCF calculation. For both of the  $\pi$  states ( $^5, ^7\Pi$ ) broken symmetry calculations were performed, i.e. in  $C_{2v}$  symmetry the two  $\pi$  symmetries were not restricted to remain equivalent. This was due to computation difficulties. However the separation between the various states was much larger than the expected energy lowering due to symmetry breaking. The small MCSCF calculations for the  $^5\Pi$  state had 6 electrons distributed among the 5 Cr3d orbitals and the 0  $2p\pi_x$  orbital, and the larger calculation had 8 electrons and the  $2p\pi_y$  orbital is also included.

For CrO at the MCSCF/SCF level the state ordering is  $^5\Pi$  (ground state),  $^7\Pi$ ,  $^5\Sigma^+$ ,  $^7\Sigma^+$ . At the CI level the ordering of the upper states is the same and it is expected that the  $^5\Pi$  will remain the ground state (calculations are in progress). For the  $^5\Sigma^+$  state  $r_e$  changes from  $3.51a_0$  for the small MCSCF to  $3.30a_0$  for the larger MCSCF and to  $3.18a_0$  at the CI level. The inclusion of excitations from the  $02p\pi$  orbital has a dramatic effect on the shortening of the bond length. At all levels of calculation near equilibrium the d population was  $\sim 4.9$ . The net charge was  $\sim 0.8$  and the overlap was  $\sim 0.45$ . The two high spin states  $^7\Sigma^+$  and  $^7\Pi$  both had considerably longer bond lengths  $\sim r_e = 3.5a_0$ , which remained essentially unchanged from SCF to CI levels. For both levels of theory the d population was approximately 4.2, and the charge was  $\sim 0.7$  at the SCF and  $\sim 4.3$  and  $\sim 0.6$ , respectively, for CI. The  $^5\Pi$  (which is still uncompleted) has an  $r_e \sim 3.4a_0$  for the small MCSCF space, with a charge of  $\sim 0.6$  and a d population of  $\sim 4.3$ . The tendency of these states to have a large  $d^4$  character is surprising considering the reasonably large  $d^5-d^4s^1$  separation, and is a question yet to be resolved.

Adsorption of CO on Al and Ni:  $\text{Al}_x\text{CO}$ ,  $\text{Ni}_x\text{CO}$

---

To study the adsorption of CO on metals a cluster model approach was employed. With this method a system of atoms (cluster) is constructed which models many of the short range properties of the bulk system. While this technique gives reliable information on the equilibrium geometry of the adsorbate relative to the substrate, as well as the vibrational frequencies, information on bond strengths is qualitative at best, however useful information on relative bond strengths can often be obtained. In these calculations the metal atoms were fixed at the bulk geometry and only the adsorbate-substrate distance was varied. In the present studies only one adsorbate molecule was present. Future studies hope to include several adsorbate atoms where the effects of lateral interactions between the adsorbates can be investigated. These effects are important in understanding the differences between high and low adsorbate coverages. In these initial studies there were two main interests, 1) to understand the role of the s, p, and d electrons in the bonding and 2) to study the effect of varying cluster size and shape on the bonding (both in terms of nature and energy). The cluster we designed to study the effects of having neighbors in the same layer only, having lower neighbors only, and then both effects competing simultaneously. In both systems only the (100) face and top sites are considered.

Both Al and Ni are face center cubic metals with lattice spacings of 4.05Å and 3.52Å, respectively. For both systems 3 clusters were considered: 1) a single metal where there were no neighbor effects, 2) a five metal atom cluster which had one atom on the top layer and 4 lower neighbor atoms (1,4) [for Al a second 5 atom cluster was also considered which had 5 atoms in the top layer (5,0)], and 3) a nine atom metal cluster which had 5 atoms in the top layer and 4 in the lower layer. For the Al clusters central atoms were all electron with a (4,3) CGTO basis and the neighbors used a 3 electron ECP with a (2,1) contracted basis. For the Ni cluster the central atom was all electron using Wachter's basis with p's and diffuse d (8s6p4d). The neighbors used Goddard's one electron

MEP with a (2,1) contracted basis. The C and O basis sets were (4,3) CGTO's for the Al clusters and (4,2) CGTO's for the Ni clusters.

For the Ni clusters the results were NiCO  $^3\Delta$  (with 4  $sp\sigma^1$ ) unbound, Ni<sub>5</sub>CO (1,4) weakly bound and Ni<sub>9</sub>CO (5,4) unbound. In all clusters the CO  $\pi$ -backbonding (metal  $\pi$  electrons being donated to the CO) was  $\sim 0.15$ . However only in Ni<sub>5</sub>CO was there substantial Ni 4p $\pi$  character, and in keeping with the model of valence  $\pi$  population aiding in the bonding, this is the only cluster which is bound. The cluster shape, 1 top 4 bottom, is consistent with the idea that the lower layer helps to reduce the sigma character by pulling it out of the way, whereas this cluster has no top neighbors to compete for the  $\pi$  electrons and hence they can aid in bonding with the CO.

For the Al cluster only those clusters which had had a large 3p $\pi$  character and a reasonably small  $\sigma$  character were bound. These include states of AlCO, Al<sub>5</sub>CO (1,4) and Al<sub>9</sub>CO (5,4). For a given cluster differing electronic configurations could lead to the CO being either bound or unbound depending upon the balance between the  $\sigma$  and  $\pi$  effects.

Thus for both systems the role of the valence sp electrons appears to be understood, however although the d's are certainly involved in the bonding of the CO to the Ni cluster their exact role is not yet clear.

Finally for NiCO it has been observed that the inclusion of correlation has a considerable effect on the bonding, and it is hoped that these effects can be observed for larger clusters at a future date.

### The Chemisorption of Oxygen on Cu and Ni (100)

The first phase of this work has involved the investigation of the diatomics NiO and CuO. The goal was to determine the extent of d involvement in these chemical bonds. This would determine the level of treatment required for the clusters. We found that there was little direct d involvement in the bonding, however their effect was to occupy space and indirectly influence the oxygen atom bonding by overlap effects. For Ni there was a little more direct d involvement than in Cu. In light of the small d involvement, the d electrons were deleted from the Ni atom and small clusters of Ni atoms were used to model the surface. For the Cu atom an all-electron treatment was used as a further calibration of the elimination of the electrons. A report of this work is summarized in the attached manuscript.

N 86 - 29 925

IN 25

D1-

97

THE NATURE OF CHEMISORBED OXYGEN ON Ni(100) AND Cu(100)

Charles W. Bauschlicher, Jr\* and Stephen P. Walch

P4097681 Polyatomics Research Institute\*\*  
Mountain View, California 94043

18310

18316

Paul S. Bagus and C. R. Brundle

IBM Research Laboratory  
San Jose, California 95193

1A 056249

**ABSTRACT:** Model calculations indicate two low-lying states for the interaction of O with Ni and Cu(100). The "oxide" state is  $\approx 1$  eV more stable and its  $R_L$  for Ni(100) is consistent with the experimental value for Ni(100), indicating only one type of stable chemisorption bond. This agrees with XPS and EXAFS data for the observed LEED structures. Interpretations of EELS data in terms of a radical state for the  $p(2 \times 2)$  and the oxide state for the  $c(2 \times 2)$  structure must be seriously questioned.

\*Present Address: NASA Ames Research Center, Moffett Field, California 94035.

\*\*Mailing Address: 1101 San Antonio Road, Suite 420, Mountain View, California 94043.

Upton and Goddard (UG),<sup>1</sup> using a 20 atom cluster to model the (100) surface of Ni, have shown that two low-lying electronic states exist for the  $\text{Ni}_{20}\text{O}$  cluster. One, termed the "oxide" state<sup>2</sup> has all oxygen orbitals doubly occupied either as lone pairs or as covalent Ni-O bonds. The other, the "radical" state, has one singly occupied  $\sigma$  orbital. On the basis of their results, UG and later Rahman, Black and Mills (RBM)<sup>3</sup> accounted for the EELS spectra of  $p(2 \times 2)\text{O}$  and  $c(2 \times 2)\text{O}$  on Ni(100) in terms of the  $p(2 \times 2)$  structures involving the "radical" state with the equilibrium distance,  $R_{\perp} \approx 0.9\text{\AA}$  and the  $c(2 \times 2)$  structure involving the "oxide" state with  $R_{\perp} \approx 0.26\text{\AA}$ . In this communication we investigate theoretically the two states on model Ni(100) and Cu(100) surfaces. Our results and comparison to existing experimental data, with the exception of the EELS interpretation, lead us to conclude that there is only one stable chemisorption bond for O on Ni(100), the "oxide" state, with  $R_{\perp} \approx 0.89\text{\AA}$ .

We model the (100) surface as a two layer, 5 atom cluster with 4 atoms in the top layer. The distance of the O atom above the 4-fold site is varied. For Ni we used the same modified effective potential (MEP)<sup>4</sup> as UG. Thus, only one Ni electron is explicitly included in the calculation, the remaining 27, including the 3d shell, are present only in the one electron potential. The contracted Gaussian type orbitals (CGTO) representing the Ni contains 2s and 1p functions. The p function is chosen to represent the Ni 4p orbital. The CGTO basis for O was (4s3p).<sup>5</sup> It contains a diffuse p function and can represent both O and  $\text{O}^-$ . For  $\text{Cu}_5\text{O}$ , we used an all electron treatment. The O basis set is optimized for  $\text{O}^-$  (4s3p) and the Cu is better than double zeta in the 3d, 4s and 4p valence region. All basis sets are adequate to represent the electron distributions rather well. Symmetry and equivalence restricted self-consistent-field (SCF) methods were used to evaluate the

wavefunctions. Correlation is included through the method of configuration interaction (CI) and includes all single and double excitations from the SCF reference.

The adequacy of the 5 metal atom clusters were tested by comparing to the  $\text{Ni}_{20}\text{O}$  results of UG. UG used only two s functions for Ni, so for comparison we deleted the Ni 4p functions. The "radical" state of  $\text{Ni}_5\text{O}$  in  $C_{4v}$  symmetry is  $^4B_2, \dots 3a_1^2 4a_1^1 1e^4 2e^2$ . The "oxide" state is  $^2E, \dots 3a_1^2 4a_1^2 1e^4 2e^1$ . The results of our SCF calculations at the equilibrium distance,  $R_1$ , of O above the  $\text{Ni}_4$  square, the energy separation of the "oxide" and "radical" states,  $\Delta E$ , and the calculated O vibrational frequency,  $\omega_e$ , are summarized in Table I. The results of UG, Walch and Goddard (WG)<sup>6</sup> and the experimental EELS frequencies<sup>7</sup> and LEED  $R_1$ 's are also given. Agreement of our  $\text{Ni}_5\text{O}$  calculations without the 4p functions with UG is very good. When, however, we put the 4p functions back into the calculations,  $R_1$  increases by  $0.11\text{\AA}$  (Table I) bringing it and the resultant  $\omega_e$  into agreement with the earlier calculation of WG on  $\text{Ni}_5\text{O}$ . We conclude that the major difference between UG  $\text{Ni}_{20}\text{O}$  and WG  $\text{Ni}_5\text{O}$  is the lack of the important 4p's in UG and not a cluster size effect. This is consistent with our previous finding<sup>9</sup> that the 4p's contribute  $\approx 50$  percent of the cluster bond energy and our view that  $R_1$ ,  $\omega_e$  and the qualitative nature of the bonding all converge rapidly with cluster size. Note also that with the 4p's included,  $\Delta E$  is only 0.1 eV.

To test whether the two states of oxygen are unique to Ni, we investigated  $\text{Cu}_5\text{O}$ . Since an all electron calculation was performed, it also serves as a check on the MEP approximation. We find the same two O states separated by a small  $\Delta E$  and conclude that they are not unique to Ni and not an artifact of the MEP approximation.

A Mulliken population analysis for our  $\text{Ni}_5\text{O}$  (no 4p) cluster shows that the "radical" state has an oxygen charge of 0.67 and the "oxide" state has a charge of 1.32 in agreement



with UG. It is also well known that at the SCF level the computed electron affinity is  $-0.54 \text{ eV}^{10}$ , far from the experimental value of  $+1.462 \text{ eV}^{11}$ . When correlation is included the electron affinity for O improves to  $+0.74 \text{ eV}$  in our basis set. When we include correlation in our  $\text{Ni}_5\text{O}$  calculation, we find that the energy of the "oxide" state drops relative to the "radical" state by  $0.79 \text{ eV}$  to give a  $\Delta E$  of  $0.89 \text{ eV}$  (Table I). This is anticipated because the large charge on the O atom in the oxide state should result in a larger correlation improvement. We also know that since we are computing only about half the experimental electron affinity of O at this level, further correlation improvements would lower the "oxide" state even further with respect to the "radical" state.

One significant difference between the  $\text{Ni}_5\text{O}$  and  $\text{Cu}_5\text{O}$  oxide state results is the  $R_1$  value,  $0.74 \text{ \AA}$  for Ni and  $\approx 0.98 \text{ \AA}$  ( $0.92 \text{ \AA}$  calculated SCF +  $0.06 \text{ \AA}$  estimated for correlation) for Cu. For all-electron calculations on the diatomics NiO and CuO, we find<sup>12</sup> almost identical bond-lengths with the computed value  $\approx 0.1 \text{ \AA}$  longer than experiment (CuO). We also find that the MEP treatment for NiO gives a value  $\approx 0.2 \text{ \AA}$  shorter than the all-electron treatment. We therefore confidently expect that in the clusters the MEP calculated Ni-O bond length in the "oxide" state will be too short and the all-electron Cu-O bond length too long. Averaging the two computed values (Ni and Cu) to give identical Ni-O and Cu-O bond lengths, as is found for the diatomics, results in  $R_1$ 's of  $0.89 \text{ \AA}$  (Ni) and  $0.82 \text{ \AA}$  (Cu). The final conclusions from our calculations for  $\text{Ni}_5\text{O}$  are, therefore, that  $R_1$  is  $\approx 0.90 \text{ \AA}$  for the "oxide" state and it is  $\geq 0.89 \text{ eV}$  more stable than the radical state.

UG suggested that the  $p(2 \times 2)\text{O Ni}(100)$  LEED structure represented formation of the "radical" O state on the surface because of agreement between their "radical"  $R_1$  and the LEED determined value ( $0.9 \text{ \AA}$ ) and because the calculated "radical"  $\omega_e$  was closer to the observed FELS vibrational frequency<sup>7</sup> than that for the "oxide". Note that this choice is

ORIGINAL PAGE IS  
OF POOR QUALITY

made primarily because of the short  $R_1$  calculated for the "oxide" by UG. We, however, find that the inclusion of the 4p functions, correlation, and an MEP bond length correction yield an "oxide" state with  $R_1$  in agreement with experiment for the  $p(2 \times 2)O$  structure in addition to the  $\approx 1$  eV greater stability of the "oxide" state. Our calculated  $\omega_e$  values for the "oxide and "radical" states are practically identical when the 4p and CI are included (Table I), though there is a large difference between the two without the 4p and CI.

UG attempted to simulate the higher oxygen coverage  $c(2 \times 2)O$  structure in their  $Ni_{20}O$  cluster by removing a charge from the cluster. This shortened the "oxide" state  $R_1$  even further (to  $0.26 \text{ \AA}$ ) ~~and gave a reduced  $\omega_e$~~  and also gave an  $\omega_e$  reduced relative to the "radical" state in agreement with the large reduction observed for the  $c(2 \times 2)O$  on  $Ni(100)$ .<sup>7</sup> UG therefore suggested that the higher coverage  $c(2 \times 2)O$  structure involved a drastic shortening of  $R_1$  and a switch to the "oxide" O state. RBM supported this opinion, since they were able to obtain a good fit to the experimental EELS vibrational frequencies using UG's  $\omega_e$  values as input parameters for their lattice dynamical calculations.

The interpretations of UG and RBM cast doubt on the LEED determined  $R_1$  for the  $c(2 \times 2)O$  structure,<sup>8</sup> which is  $\approx 0.9 \text{ \AA}$ , identical to the  $p(2 \times 2)O$ .<sup>8</sup> It is certainly true that the LEED data for  $c(2 \times 2)O$  and its fit to theory are poor and should be remeasured. There are however, several other experimental measurements which indicate that only a single type of O chemisorption state exists over the entire adsorption range up to oxide nucleation (at  $\approx 0.38$  monolayers).<sup>13</sup> XPS shows only one O(1s) B.E. for the  $p(2 \times 2)O$  and  $c(2 \times 2)O$  structures.<sup>14</sup> Our orbital energies would imply a 1.6 eV B.E. difference between oxide and radical states at their equilibrium  $R_1$  values, and still 1.2 eV for the oxide state at a  $R_1$  as short as  $0.4 \text{ \AA}$ . The work function increase as a function of coverage shows only a smooth increase over the entire chemisorption range, indicating the presence of only one type of

O.<sup>15</sup> Finally, recent EXAFS data<sup>16</sup> demonstrates both from adsorption edge characteristics and from EXAFS structure that the oxygen atoms in the  $p(2 \times 2)$  and  $c(2 \times 2)$  structures are identical in electronic character and  $R_{\perp}$ . Their EXAFS derived value for  $R_{\perp}$   $0.86 \pm 0.07 \text{ \AA}$  is in excellent agreement with our estimated value of  $0.90 \text{ \AA}$  for the "oxide" state.

We conclude that both the theory and experimental data for the  $\text{Ni}(100)/\text{O}$  system indicate that only one stable chemisorption state, the "oxide" state, exists and that  $R_{\perp}$  for the state is  $\approx 0.9 \text{ \AA}$ , as proposed in the original LEED data. We also predict that for  $\text{Cu}(100)$ , oxygen will sit  $\approx 0.83 \text{ \AA}$  above the surface. We feel that the  $\text{Ni}_{20}\text{O}^+$  calculations of UG rather than simulating the  $c(2 \times 2)\text{O}$  structure is actually simulating oxide nucleation; hence the extremely short  $R_{\perp}$  produced. The EELS data showing a large decrease in O vibrational frequency on going from  $p(2 \times 2)\text{O}$  to  $c(2 \times 2)\text{O}$  remains unexplained. Either there is some problem with the data, possibly involving some unrecognized oxide nucleation, or the claims<sup>3</sup> that merely increasing O coverage without changing  $R_{\perp}$  cannot, theoretically, result in the observed frequency decrease are incorrect. We note that the experimental EELS changes on going from  $p(2 \times 2)\text{O}$  to  $c(2 \times 2)\text{O}$  are rather complex and continuous. Theoretically, we are directly investigating the effect of neighboring O's on  $\omega_e$  by placing several O's on a large Ni cluster. Finally, with respect to the "radical state," we feel that it is a genuine low-lying state, but not the ground state at any coverage. It may have importance as an intermediate during reactions on Ni or Cu surfaces.

ORIGINAL PAGE IS  
OF POOR QUALITY

TABLE I

Summary of Results

Calculation/ Experiment	Radical State		Oxide State		$\Delta E(\text{eV})$
	$R_{\perp}(\text{\AA})$	$\omega_e(\text{cm}^{-1})$	$R_{\perp}(\text{\AA})$	$\omega_e(\text{cm}^{-1})$	
UG $\text{Ni}_{20}\text{O}^a$	0.88	371	0.55	218	0.34
RBM <sup>b</sup>		445			
UG $\text{Ni}_{20}\text{O}^+{}^a$	0.83	355	0.26	266	1.03
RBM <sup>b</sup>				295	
WG $\text{Ni}_5\text{O}^c$			0.65	290	
WG $\text{Ni}_5\text{O}^+{}^c$	0.96	300			
THIS WORK					
$\text{Ni}_5\text{O}$ (no 4p)	0.87	374	0.57	251	0.42
with 4p	0.98	358	0.68	290	0.10
with 4p and CI	0.91	317	0.74	320	0.89
$\text{Cu}_5\text{O}$ SCF only	1.37 <sup>d</sup>	280	0.92	330	0.21
EXPERIMENT					
$p(2 \times 2)\text{O Ni}(100)$			$\sim 0.90^e$	430 <sup>f</sup>	
$c(2 \times 2)\text{O Ni}(100)$			$\sim 0.90^e$	310 <sup>f</sup>	

<sup>a</sup>Ref. 1.<sup>b</sup>Ref. 3, using the  $\omega_e$  in the line above as the single particle input parameter.<sup>c</sup>Ref. 6. The  $\text{Ni}_5\text{O}$  calculation converged on the "oxide" state and we assume the  $\text{Ni}_5\text{O}^+$  calculation converged to the "radical" state.<sup>d</sup>Average of configurations used for the "radical" state<sup>e</sup>Ref. 8,  $R_{\perp}$  determined from the theoretical fit to IV curves.<sup>f</sup>Ref. 7, frequency of major peak, assumed to be surface-O stretch.

## REFERENCES

1. T. H. Upton and W. A. Goddard, Phys. Rev. Lett **46**, 1635 (1981), and T. H. Upton and W. A. Goddard, "Critical Reviews in Solid State and Material Sciences," CRC Press (1981).
2. We consider "oxide" state a poor name, since this is actually a chemisorbed oxygen state with no open shell electrons, and is not to be confused with the oxide formed through nucleation of the surface at high oxygen coverages. We use it, however, to be consistent with Refs. 1 and 3.
3. T. S. Rahman, J. E. Black and D. L. Mills, Phys. Rev. Lett. **46**, 1469 (1981).
4. C. F. Melius, C. L. Bisson and W. D. Wilson, Phys. Rev. B **18**, 1647 (1978). MEP, exponents and coefficients taken from Table VI with the following corrections  $V_{s-d}$   $a_i$  changed from -0.085 to -0.85 and alpha 0.1982 changed to 0.9182.
5. T. H. Dunning and P. J. Hay, "Modern Theoretical Chemistry, Vol. 3," ed. H. F. Schaefer, (Plenum Press, New York, 1977. Their DZ contraction plus their O<sup>-</sup> function.
6. S. P. Walch and W. A. Goddard, Surf. Sci. **75**, 609 (1978).
7. S. Lehwald and H. Ibach, Vibrations at Surfaces, ed. R. Caudano, J.-M. Guilles and A. A. Lucas (Plenum, New York, 1982), p. 137.
8. M. Van Hove and S. Y. Tong, J. Vac. Sci. Technol. **12**, 230 (1975); P. M. Marcus, J. E. Demuth and D. W. Jepsen, Surf. Sci. **53**, 501 (1975).
9. B. N. Cox and C. W. Bauschlicher, Surf. Sci. **108**, 483 (1981).
10. Numerical Hartree-Fock yields 0.54 eV, 0.58 eV in our basis.
11. H. Hotop and W. C. Lineberger, J. Phys. and Chem. Ref. Data. **4**, 530 (1975).

12. P. S. Bagus, C. J. Nelin and C. W. Bauschlicher; and C. W. Bauschlicher, S. P. Walch and P. S. Bagus, unpublished work as compared to S. P. Walch and W. A. Goddard, *J. Amer. Chem. Soc.* **100**, 1338 (1978).
13. See for example, C. R. Brundle in "AIP Conference Proceedings Number 61," ed. U. Landman, AIP, New York (1981).
14. C. R. Brundle and H. H. Hopster, *J. Vac. Sci. Tech.* **18**, 663 (1981). Initially, it was thought that two states might exist at low temperatures, but it has since been shown that the second state represents a carbonate impurity (R. J. Behm and C. R. Brundle, to be published).
15. P. H. Holloway and J. B. Hudson, *Surf. Sci.* **43**, 123 (1974).
16. J. Stohr, R. Jaeger and T. Kendelewicz, submitted to *Phys. Rev. Lett.*

The following is the final report of Dr.C.J. Nelin who was the principal investigator on this grant from July 1982 through January of 1983. Dr. Nelin had to leave this project since NASA Technical personel did not wish to continue to fund further work on this grant.

This report provided interim status on this grant, and was submitted to NASA Technical personel in April of 1983.

N86 - 29926

1N-25

D2

289.

18316

A FINAL REPORT ON THE EXTENSION OF THE MCSCF/CI METHOD

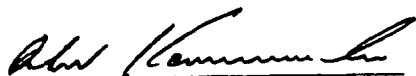
Polyatomics Proposal: NASA Ames Cooperative Agreement NCC2-158

Prepared by: Constance J. Nelin  
Polyatomics Research Institute  
1101 San Antonio Road, Suite 420  
Mountain View, CA 94043

PP097681

Submitted to: NASA Ames Research Center  
Moffett Field, CA 94035

Date: April 8, 1983



Andrew Komornicki

Director



## Part I. Introduction

For the period of July 1982 through January 1983, the research carried out under this grant has focused on the nature of metal adsorbate bonding. Two main areas were investigated in detail: 1) the adsorption of CO on Al, Na, Mg and Ni and 2) bonding in transition metal oxides, CuO, CrO and MoO. These theoretical studies have lead to a new understanding of CO-metal bonding as well as to a better understanding of the d involvement in the bonding in transition metal oxides. The research carried out, while useful in itself for the understanding gained, also serves as a calibration of the methods employed. This is necessary information if these methods are to be later applied to other systems.

Part of this work has been accepted for publication and copies of the two papers are given in Appendices A and B. Other parts have been given as presentations at various meetings. This work was done in collaboration with Paul S. Bagus (IBM Research Laboratory) and Charles W. Bauschlicher, Jr. (NASA Ames Research Center).

This report is structured in three parts. Part II discusses the cluster model studies. Four areas are discussed in detail: hybridization and charging in cluster model studies, the adsorption of CO on metals (Al, Na, Mg), the adsorption of CO on Ni, and finally the use of Effective Core Potentials (ECP) in cluster model studies. In Part III the study of transition metal oxides, in particular CrO, MoO and CuO, is discussed.

## Part II. Cluster Model Studies of Metal-Metal and Metal-Adsorbate Interactions

### A) Introduction

To study the nature of metal-metal and metal-adsorbate interactions a cluster model approach was employed. For this technique a bulk system is modelled by the use of a system of atoms (a cluster) which is constructed in such a way that it accurately predicts many of the local properties of the bulk system. While this technique gives reliable information about the equilibrium geometry of the adsorbate relative to the substrate, the vibrational frequencies, and the bonding mechanisms, detailed information on bond strengths is only qualitative in nature. Due to the finite size of the cluster, the metal atoms are held fixed at the bulk geometry and only the adsorbate-surface distance is allowed to vary.

The primary emphasis of this study was to gain a better understanding of the mechanisms of CO-metal bonding. However we also analyzed the extent to which finite cluster effects (artifacts) can affect the calculation. Both the effects of changing the cluster size (number of atoms) and shape (inclusion of neighbors, next nearest neighbors, etc.) were investigated in detail.

In part B of this section the nature of cluster effects as demonstrated through charging and hybridization will be discussed briefly. This work has been accepted by Chemical Physics Letters and the details are given in the attached paper (Appendix A). In parts C, D, and E the nature of CO-metal (Al, Na, Mg), CO-Ni bonding, and the effects of ECP's will be discussed.

### B) Charging and Hybridization in the Finite Cluster Model

For a cluster to accurately model the interaction of an adsorbate with a solid surface, the cluster wavefunction should have appropriate hybridization and polarization (i.e. close to that for the bulk material). To study the effect of cluster size on charging and hybridization

clusters of Be, Mg and Al were investigated. It had been thought previously that when all of the bonding site atoms have their nearest neighbors then  $r_e$ ,  $\omega_e$  and the nature of bond of an adsorbate to this cluster would be effectively converged. This rule of thumb appears to be true for the Mg and Be clusters, where for  $\text{Be}_{10}$  and  $\text{Mg}_{10}$  the three types of atoms in the cluster, central, first layer edge and second layer are all essentially neutral. However for  $\text{Al}_{10}$  the central atom is negatively charged by 0.63 electrons. When the size and shape of the Al cluster was changed ( $\text{Al}_5$ ,  $\text{Al}_{13}$ ) there were further dramatic changes in the charging. It was also seen that the hybridization of the central atom is dependent on the cluster size and shape, eg. for Mg the hybridization as measured by the 3p population changes from 0.22 for  $\text{Mg}_4$  to 0.85 to  $\text{Mg}_{13}$ . However in Al there is similar central atom hybridization in  $\text{Al}_5$ ,  $\text{Al}_{10}$  and  $\text{Al}_{13}$  cluster.

Although it would be nice to have rules for the design of "good" clusters, it is now clear that the magnitude of finite cluster effects varies from material to material and even for clusters chosen to represent different faces of a crystal or different adsorption sites. Thus it appears necessary to investigate the question of appropriate cluster size separately for each chemisorption problem. More detail of this study is given in the attached paper (Appendix A).

### C) The Bonding of CO to Metal Surfaces

The commonly accepted idea of the bonding of CO in metal carbonyls is one of  $\sigma$  donation and  $\pi$  back-donation<sup>1</sup>. The CO is oriented with C toward the metal atom and the CO  $5\sigma$  (C lone pair) orbital donates charge to and bonds with the metal. This  $\sigma$  donation leads to a back-donation into the unoccupied CO  $2\pi^*$  level which is also bonding. Angular dependent photoemission spectroscopy (PES) studies of CO on several transition metals (see Ref. 2 and references therein) have been interpreted to show that the molecular axis of the adsorbed CO is normal to the surface with C nearest the metal. Low energy electron diffraction (LEED) studies for CO/Ni(100) and CO/Cu(100) have further shown that CO is in a head-on site directly on top of a surface atom<sup>3</sup>. For CO adsorbed

in this geometry the interpretation of the bonding, based on both theoretical<sup>4</sup> and experimental results<sup>2</sup>, is the same as for the metal carbonyls, i.e.  $\sigma$  donation and  $\pi$  back-donation. In photoemission, ionization of the CO  $5\sigma$  derived orbital, for CO/Ni and on other surfaces, shifts to a higher binding energy (BE) relative to the CO  $1\pi$  level<sup>2, 4-6</sup>; these two levels of adsorbed CO have essentially the same BE. This has been taken as evidence that this CO  $\sigma$  level is significantly, or even primarily<sup>2</sup>, involved in the bonding of CO to the surface. Theoretical studies have suggested that both the metal valence sp and the d electrons are involved in the metal to CO bonding<sup>4,6,7</sup>.

In order to separate the effects due to the d and the sp electrons, we consider model studies of the interaction of CO with Na, Mg, and Al; they are all metals which do not have occupied d shells. In the next part the effects of d electrons will be discussed through the study of CO/Ni. Since we wish to apply our analysis to metals where the chemisorption of CO has been studied rather extensively, we use the normal, head-on site geometry for CO as established for Ni, Cu, and other transition metals. The atoms treated differ primarily in the number of valence electrons but also in the symmetry character, 3s or 3p, of these electrons. The results are based on ab initio SCF cluster calculations for the interaction of CO with either one or four metal atoms; the clusters are denoted XCO and  $X_4(1,3)CO$  where X=Na, Mg, or Al. For each of the linear XCO clusters, we have considered two states: 1) a state with  $\Sigma^+$  total symmetry where all the metal valence electrons have  $\sigma$  symmetry, and 2) a state with  $\Pi$  total symmetry where one of the metal valence electrons has  $\pi$  symmetry. Thus we have one case, state (1), where there is no  $\pi$  interaction possible between the metal and CO and a second case, state (2), where this  $\pi$  interaction is possible. By comparing the bonding in these two states we can more easily distinguish the nature of the interactions in  $\sigma$  as opposed to  $\pi$  symmetry. The  $X_4(1,3)CO$  clusters are chosen to simulate adsorption on the (1000) face of a hexagonal close packed (hcp) structure for Na and Mg and the (111) face of face-centered cubic (fcc) Al. The  $X_4(1,3)$  clusters contain one first layer atom, the adsorption site, and its three nearest neighbors in the second layer of the crystal.

In these clusters there is a natural hybridization of the surface metal atom's electrons into  $\sigma$  and  $\pi$  character relative to the CO axis; hence both types of interaction with the CO are possible. Polarization of the charge associated with the surface metal atom, either toward or away from the CO, is also possible and this may affect the nature of the interaction. For both the XCO and  $X_4$ CO clusters the distance of CO from the surface metal atom has been varied and the interaction has been studied as a function of this distance.

Our analysis of the results of these cluster calculations leads to an interpretation of the bonding of CO which is quite different from the generally held view. We find that the interaction in the  $\sigma$  space is rather repulsive. A corresponding orbital analysis<sup>8,9</sup> shows that the orbitals of free CO are also, to a very large extent, occupied in the cluster, XCO or  $X_4$ CO, wavefunctions. Thus there is very little, if any,  $\sigma$  donation from CO to metal. We do, however, find that the metal charge in  $\sigma$  symmetry hybridizes and polarizes away from CO so as to reduce the metal with CO  $5\sigma$  overlap and hence to reduce the repulsion. The interaction in the  $\pi$  space is by contrast, quite attractive. The corresponding orbital analysis<sup>8,9</sup> shows that there is often a considerable transfer of charge from the metal  $\pi$  electrons to CO and this is supported by the results of a more usual population analysis<sup>10</sup>. In the case of the  $X_4(1,3)$  CO clusters, there is a competition for the bonding character of the  $\pi$  electrons associated with the surface metal atom. These electrons (less than one) can bond this atom to the CO or they can bond it to the second layer metal atoms. In the later case the  $\pi$  electrons contribute to the stability of the cluster (or the crystal surface which is being modelled) rather than to the stability of the adsorbed CO. The strength of the metal-CO bond can be related to the amount of  $\pi$  charged transferred from metal to CO  $2\pi^*$ . The net bonding of CO to the metal is the result of the sum of the  $\sigma$  repulsion and the  $\pi$  attraction.

Thus we characterize the metal-CO bonding as a  $\pi$  donation from metal to CO  $2\pi^*$  coupled with a  $\sigma$  polarization to reduce the repulsion in this space. Studies in progress indicate that this description of the bonding

applies for the interaction of CO with transition metals as well as for the simple metals discussed here. These studies will be reported elsewhere<sup>11,12</sup> when they are completed.

We have also examined BE shifts for the cluster levels derived from CO  $5\sigma$ ,  $1\pi$ , and  $4\sigma$ . We find that there is a large initial state shift of the  $5\sigma$  derived level to higher BE even for systems and metal-CO distances where the net interaction is quite repulsive. This shift is a consequence of the interaction and mixing of the metal and CO orbitals of  $\sigma$  symmetry. However, it is not possible to relate the  $5\sigma$  derived BE shift to the strength of the chemical bond formed between the metal and CO as has been attempted in the past<sup>2</sup>. In particular we show that our results for AlCO and Al<sub>4</sub>CO are consistent with the two peaked structure observed in the He I PES for low coverage of CO on Al(111) by Schmeisser et al.<sup>13</sup>. Thus, even for the weakly bound adsorption of CO/Al<sup>14</sup>,  $\sim 0.21\text{eV}$ /molecule, it may indeed be the case that CO adsorbs normal to the surface at a head-on site.

#### D) Adsorption of CO on Ni(100)

In the study of CO bonding to metals (Al, Na, Mg) we found that the dominant effect of the  $\sigma$  electrons is repulsion whereas the bonding occurred in the  $\pi$  space. We were then interested to see if this mechanism also applied to systems where d electrons were present. We hoped to find out what, if any, was the role of the d electrons in the bonding. Once again we are considering bonding to a head on site. The clusters studied were designed such that we could see the effects of having no substrate neighbors, NiCO, lower layer neighbors only, Ni<sub>5</sub>(1,4)CO, and finally both lower and top layer neighbors, Ni<sub>9</sub>(5,4)CO. It is expected that CO would bond more strongly to the Ni<sub>5</sub> than to the Ni<sub>9</sub> cluster as in the Ni<sub>5</sub> cluster the lower layer Ni atoms would tend to polarize the  $\sigma$  electrons downward, hence reducing the repulsion and there would not be the competition for the  $\pi$  electrons between the CO and the neighboring surface atoms which would exist in the Ni<sub>9</sub> cluster. There may also be different charging of the central atom (the adsorption) site which could effect the bonding. For

the clusters the Ni atoms are fixed at bulk Ni lattice spacing, 3.52Å, the Ni-CO distance is 1.84Å [the Ni-CO distance for Ni(CO)<sub>4</sub>] and the C-O distance is 1.15Å (the C-O distance for free CO). In these clusters the adsorption site was treated as an all electron atom, and the neighboring atoms used 1 electron ECP's. (This approximation is discussed in more detail in Part E.) The basis sets used, contracted gaussian type orbitals (CGTO), were [8,6,4] for the all electron Ni, [2,1] for the ECP Ni and [4,2] for the C and O.

#### NiCO

Once again we were able to form two types of states, one with Ni 3d<sup>9</sup>4spσ<sup>1</sup> (<sup>3</sup>Δ) and the other with Ni 3d<sup>9</sup>4pπ<sup>1</sup> (<sup>3</sup>Φ). There is, however, a fundamental difference between these two states and those formed for the simple (non-transition) metal-CO (Al, Na, Mg). In the <sup>3</sup>Δ state although there is no possible 4pπ → 2π\* bonding, it is now possible to have dπ → 2π\* bonding occur. For the <sup>3</sup>Δ state there is π bonding, e.g. the CO π population is 0.11, however there is a comparable amount of repulsion. The net result is that the state is slightly unbound E = -0.09eV. On the other hand for the <sup>3</sup>Φ state, where both 4pπ → 2π\* and dπ → 2π\* bonding is possible, we find CO(π) = 0.68 and ΔE = 1eV. Thus while dπ → 2π\* may contribute to the bonding 4pπ → 2π\* is still the dominant bonding mechanism.

#### Ni<sub>5</sub>(1,4)CO

The Ni<sub>5</sub> cluster is constructed with one Ni atom in the top layer (all electron) and four lower layer Ni atoms (ECP). The state we consider has a d δx<sup>2</sup>-y<sup>2</sup> hole, however the different d holes in the σ and δ space are all quite close in energy. As expected this state is bound, ΔE = 0.50eV, with CO(π) = 0.17. If we compare with NiCO <sup>3</sup>Δ, which was unbound, we now have the opportunity to get bonding both from the dπ and the 4pπ (on NiCO <sup>3</sup>Δ only dπ could bond). Furthermore comparing the populations of the Ni in NiCO <sup>3</sup>Δ with the central Ni in Ni<sub>5</sub>CO, we see that the 4pπ population has changed from +0.01 (NiCO) to +0.31 (Ni<sub>5</sub>CO), the pσ population has remained similar +0.30 (NiCO) to +0.31 (Ni<sub>5</sub>CO) (however now this can be and is polarized out of the way), and the s population has been considerably reduced from -0.05 (NiCO) to -0.56 (Ni<sub>5</sub>CO). Thus the repulsion has been

considerably reduced while at the same time there are more  $\pi$  electrons to become involved in the bonding. The net result being that the state is bound. Also, again, as in the simple metal-CO clusters, the valence sp electrons play a dominant role in the bonding and repulsion. Although the d electrons appear to be involved (this is best seen in NiCO) their role is by no means clear at the present time.

#### Ni<sub>9</sub>CO

In the Ni<sub>9</sub> cluster four more ECP Ni atoms have been added as top layer neighbors, resulting in five atoms in the first layer and four in the second. As before the adsorption site is an all electron Ni atom. As predicted, due to the competition for the  $\pi$  electrons, they can either bond to the CO or to the neighboring Ni atoms. CO is unbound in this cluster,  $\Delta E = -1.28\text{eV}$ . Although the CO  $\pi$  population, 0.14, is approximately the same as in NiCO <sup>3</sup> $\Delta$  and Ni<sub>5</sub>CO, the Ni p $\pi$  population, -0.08, is more like that of NiCO than that of Ni<sub>5</sub>CO.

As with the simple metal-CO we once again feel that the bonding of CO to Ni occurs in the  $\pi$  space (predominately through the Ni valence 4p, however the role of the d's is not yet established), and the  $\sigma$  space dominately provides repulsion.

#### E.) The Use of ECP's in Cluster Calculations

To treat larger clusters, especially those composed of heavy atoms, it becomes necessary to find a way to reduce the number of electrons which must be treated exactly. One technique rapidly gaining popularity is the use of Effective Core Potentials (ECP). The philosophy behind this approximation is that in heavier atoms many of the electrons are inert with respect to the chemistry occurring, and as such they can be treated by a modelled potential which provides the appropriate interactions (mostly repulsive) with other electrons.

As a part of the study on cluster effects we also examined the effects of the use of ECP's both for the entire cluster and as neighboring atoms to the adsorption site. We looked at both Al and Ni clusters.

For the Al cluster we focused on the Al<sub>4</sub>(1,3)CO cluster, (111) face. The ECP used for this study was a 3 electron ECP in which the Al 3s and 3p electrons were left as valence electrons. The results of the SCF calculations



are shown in Table I. Basically we find identical results between the all electron cluster and the cluster in which the adsorption site was all electron and the second layer neighbors were ECP's. The small differences can possibly be explained as basis set effects (i.e. the use of the ECP introduces a slightly different basis set).

A second comparison was made for the  $\text{Ni}_5(1,4)\text{CO}$  cluster, (100) face. The ECP used in this case was a 1 electron modified ECP of Goddard. In this ECP only the 4s electron was left as a valence electron and furthermore the potential was modified to give the correct Ni atomic separations. For this study three different clusters were considered, one with 5 all electron Ni atoms, one with the adsorption site an all electron Ni atom and the second layer neighbors as ECP's, and finally one in which all 5 Ni atoms, including the adsorption site, used ECP's. The results are given in Table II. Once again the two clusters in which the adsorption site was an all electron Ni atom gave very similar results. However the all ECP cluster results were extremely different, and highly unphysical. [e.g. We have found that the bonding of CO to a metal or transition metal occurs in the  $\pi$  space yet this cluster which is the most strongly bound of the three,  $D_e = 1.33\text{eV}$ , has no  $\pi$  bonding,  $\text{CO}(\pi) = 0.03!$ ] One problem with using a 1 electron ECP on the adsorption site is that the d electrons do not appear to be inert. It is probable that a cluster with a 10 electron ECP (with the 3d and 4s electron as valence electrons) used for the adsorption site would lead to more reasonable results.

From these two studies we feel that it is relatively safe to use ECP's for neighboring substrate atoms, however great care must be taken if they are to be used for atoms directly bonded to the adsorbate.

### Part III. Study of Transition Metal Oxides

#### A) Introduction

The study of selected transition metal oxides was undertaken for two key reasons: 1) The results can be calibrated by existing experimental results, or in some cases they can provide a new interpretation of the experimental results; and 2) they can provide a foundation for future studies of oxygen adsorption and oxidation of metal surfaces.

The transition metal oxides discussed in this section, CrO, MoO and CuO are part of a larger study (with C.W. Bauschlicher and P.S. Bagus) which also includes NiO, PdO, CuO and AgO. Through this study both the effect of moving across the row (varying the number of d electrons) as well as the effect of moving down the column (varying the spatial extent of the d electrons) could be analyzed. The results of this larger study are currently being organized and will be discussed elsewhere<sup>16</sup>. This report will only discuss the specific results for CuO, CrO and MoO. (CuO will only be discussed briefly; a more detailed discussion of the results is given in the attached paper, Appendix B.)

#### B) CuO - Predictions of a New Excited State

Initially we choose to investigate CuO for two reasons: 1) because Cu is the simplest transition metal to treat computationally due to its closed d shell, and 2) Huber and Herzberg<sup>15</sup> had reported the  $X^2\Pi-A^2\Sigma^+$  separation to be  $\sim 16,500\text{cm}^{-1}$ , which was considerably different from the  $\Sigma-\Pi$  separation,  $350\text{cm}^{-1}$ , of the neighboring alkali oxide KO. As such CuO was viewed to be a prime candidate for d involvement in the bonding.

We computed SCF and CI wavefunctions for the ground and several low-lying states of CuO. One expects CuO to be a very ionic molecule with essentially  $\text{Cu}^+$  and  $\text{O}^-$  character, and as such we classify the states according to their free ion states. We find the ground state of CuO to be the  $X^2\Pi$  state with  $\text{Cu}^+(3d^{10})$ , and we further find the first excited state  $2\Sigma^+$  [also  $\text{Cu}^+(3d^{10})$ ] to be located at  $\sim 8000\text{cm}^{-1}$ , a considerably different value than that given by Huber and Herzberg<sup>15</sup>. However this lower lying

excited  $^2\Sigma^+$  state has since been observed experimentally at  $7865\text{cm}^{-1}$  <sup>17</sup>.

We feel that the state reported in Huber and Herzberg was probably an excited  $^2\Sigma^+$  state arising from  $\text{Cu}^+$  in a  $3d^9 4s^1$  configuration. We predict that the states formed from  $\text{Cu}^+(3d^4 4s^1)$  will be  $10,000 - 30,000\text{cm}^{-1}$  above the ground state.

The computed separation of the  $X^2\Pi$  and lowest  $^2\Sigma^+$  is now closer to the separations obtained for the alkali oxides <sup>18</sup>. The magnitude and direction of this separation can be explained by an analysis of the integrals between orbitals of the separated free ions. The details of this analysis and further details of the calculations are given in the attached paper (Appendix B).

#### C) CrO, MoO - A Clear Case of d Bonding

In contrast to CuO where the lowest states had filled d shells, CrO and MoO can have the maximum number of open d shells. Once again the systems are expected to be highly ionic, essentially  $\text{Metal}^+$  and  $\text{O}^-$ . From the separations given in Table III we would expect that the lowest lying states would have either  $\text{Cr}^+$  or  $\text{Mo}^+$  in a  $d^5$  configuration. However this simple model (looking at the ionic components) which worked well for CuO appears to break down when there are a large number of open d shells. There is however very little experimental information available for either CrO or MoO, hence most of the results obtained will be predictive in nature.

The contracted Gaussian orbital basis for Cr is that of Wachters <sup>20</sup> including two functions to represent the 4p orbital and also including Hay's <sup>21</sup> diffuse d function (14,11,6/[8,6,4]). The oxygen basis set is based on Dunning's <sup>22</sup> double zeta contraction of Huzinaga's set including also a diffuse p,  $\alpha=0.059$ , to represent the  $\text{O}^-$  character and a d,  $\alpha=0.90$ , (9,6,1/[4,3,1]). The Mo basis set is Huzinaga's set contracted using a generalized contraction and also including a three term f function (17,13,9,3/[7,7,4,1]).

For  $\text{O}^-$ , in  $C_{\infty v}$  symmetry there are two possible states:  $\sigma^1 \pi^4$  ( $\sigma$  hole) and  $\sigma^2 \pi^3$  ( $\pi$  hole). When the  $\text{O}^-$  is combined with either  $\text{Cr}^+(3d^5)$  or  $\text{Mo}^+(4d^5)$  the resulting states are  $^5,7\Sigma^+$  and  $^5,7\Pi$ . Both of the quintet states have the possibility of bond formation. For the  $^5\Sigma^+$  state the SCF configuration would be:

$$(d\sigma + 02p\sigma)^2 d\pi^2 d\delta^2 02p\pi^4$$

and for the  $^5\Pi$  state the SCF configuration would be

$$(d\pi + 02p\pi)^2 d\pi 02p\pi^2 d\sigma^1 d\delta^2 02p\sigma^2.$$

For both CrO and MoO the high spin states,  $^7\Pi$ ,  $^7\Sigma^+$ , are treated at the SCF level followed by a single reference singles and doubles CI(SDCI).

For the other states a MCSCF approach is used followed by a multi-reference SDCI. The MCSCF approach used is the Complete Active Space SCF (CASSCF).

In this approach the active electrons are allowed to form all possible spin and symmetry allowed distributions among the active orbitals. For both the  $^5\Sigma^+$  and  $^5\Pi$  space two different active spaces were used. For the  $^5\Sigma^+$  the active spaces in  $C_{2v}$  symmetry were:

$$[3,1,1,1] - 02p\sigma, d\sigma, d\delta; d\pi; d\pi; d\delta \quad (6 \text{ electrons})$$

$$[3,2,2,1] - 02p\sigma, d\sigma, d\delta; 02p\pi, d\pi; 02p\pi, d\pi; d\delta \quad (10 \text{ electrons})$$

and for the  $^5\Pi$  state the active spaces were:

$$[2,2,1,1] - d\sigma, d\delta; 02p\pi, d\pi; d\pi; d\delta \quad (6 \text{ electrons})$$

$$[3,2,2,1] - 02p\sigma, d\sigma, d\delta; 02p\pi, d\pi; 02p\pi, d\pi; d\delta \quad (10 \text{ electrons})$$

The resulting configurations from the small CAS calculations were bonding, anti-bonding and spin-recoupling. It turns out that the spin-recoupling terms are as, if not more, important than the anti-bonding terms. Thus for these systems a GVB wavefunction which neglects the recoupling terms would give very misleading results. For both the  $^5\Pi$  and  $^5\Sigma^+$  the multi-reference SDCI is performed using the small CAS space as the reference.

It should be pointed out that due to program limitations the  $^5\Pi$  states were done in broken symmetry (i.e. in  $C_{2v}$  symmetry the two  $\pi$  symmetries were not restricted to remain equivalent), and as such were not pure  $\Pi$  states. However it is felt that the results from these broken symmetry states should well approximate those of the pure  $^5\Pi$  states.

The quintet states, especially the  $^5\Sigma^+$  for CrO, show very dramatic changes as the level of correlation increases (see Figure 1). For this CrO state, on going from the small CAS to the SDCI, the equilibrium distance shortened by 0.32Å,  $\omega_e$  changed from 420cm<sup>-1</sup> to 750cm<sup>-1</sup>, and  $D_e$  increased by 1eV. One possible interpretation of these dramatic changes is that

for the small active space only the  $d\sigma-02p\sigma$  bond was formed but then when the correlation was increased there was now also the possibility of some weak bonding in the  $\pi$  space as well. This possibility is being investigated further.

A summary of the CrO and MoO oxide results are given in Tables IV - VII and Figures 2 - 5. For CrO the state ordering at the CASSCF/SCF level is  $5\Pi$ ,  $7\Pi$ ,  $7\Sigma^+$ ,  $5\Sigma^+$  (Figure 2); for MoO the  $5\Sigma^+$  now drops below the  $7\Pi$ ,  $7\Sigma^+$  to give the ordering  $5\Pi$ ,  $5\Sigma^+$ ,  $7\Pi$ ,  $7\Sigma^+$ , (Figure 3). For both systems the CI ordering is  $5\Pi$ ,  $5\Sigma^+$ ,  $7\Pi$ ,  $7\Sigma^+$ , (Figures 4 and 5). Thus we see for MoO the  $5\Sigma^+$  state was already reasonably well described by the small CAS calculations. For both CrO and MoO we find the  $5\Pi-5\Sigma^+$  separation to be  $\sim 6000\text{cm}^{-1}$  (see Tables IV and V), which is much the same as that for CuO,  $\sim 7500\text{cm}^{-1}$ . These separations have yet to be determined experimentally. For the CrO  $5\Pi$  state experimental information is available about  $r_e$  and  $\omega_e$  and the CI results agree extremely well (see Table V). For both the  $5\Sigma^+$  and  $5\Pi$  states of CrO and MoO the dominant bond formed is a  $d-02p$  bond ( $\sigma$  or  $\pi$  respectively).

A perplexing feature of these calculations is shown in Tables VI and VII. It had been predicted that the low-lying states of CrO and MoO should be formed from  $\text{Cr}^+$  or  $\text{Mo}^+$  in a  $d^5$  configuration, however many of the states are more  $d^4s^1$  in character. A partial explanation for this effect can be seen by examining the effect of a point charge on the  $d^5-d^4s^1$  separation of  $\text{Cr}^+$ . If the energy of  $\text{Cr}^+$ , in the field of a point charge at  $r = 3.252$  a.u., is evaluated using the orbitals for a free  $\text{Cr}^+$  ion, we find that the  $d^4s^1$  state ( $d\pi^2d\delta^2$ ) drops  $74\text{cm}^{-1}$  below the  $d^5$  state. If the orbitals are allowed to relax the  $d^4s^1$  state drops even lower. Certainly representing  $\text{O}^-$  as a point charge is an approximation and also the states are not pure ionic (e.g. the  $d^4s^1$  type states of CrO and MoO have  $Q \sim 0.6$ ), however this effect certainly is part of the explanation of the  $d^4s^1$  character. It is also probable that in going from  $d^5$  to  $d^4s^1$  that the repulsion due to overlap of the Metal $^+$  orbitals with  $\text{O}^-$  orbitals is reduced. This possible effect is still under investigation.

It should be stressed that the results presented here for CrO and MoO are preliminary in nature, and the computational data is still being analyzed and interpreted.

## References

1. F.A. Cotton and G. Wilkinson, "Advanced Inorganic Chemistry", Wiley, New York 1972.
2. C.L. Allyn, T. Gustafsson and E.W. Plummer, Chem. Phys. Lett. 47, 127 (1977).
3. a) S. Andersson and J.B. Pendry, Phys. Rev. Lett. 43, 363 (1979).  
b) M. Passler, A. Ignatiev, F. Jome, D.W. Jepsen and P.M. Marcus, ibid. 43, 360 (1979).
4. P.S. Bagus, K. Herman and M. Seel, J. Vac. Sci. Technol. 18, 435 (1981) and references therein.
5. L.S. Cederbaum, W. Domcke, W. van Niessen and W. Brenig, Z. Phys. B 21, 381 (1975).
6. K. Herman and P.S. Bagus, Phys. Rev. B. 16, 4195 (1977).
7. P.S. Bagus and K. Herman, Surf. Sci. 89, 588 (1979); K. Herman and P.S. Bagus, Solid State Commun. 38, 1257 (1981).
8. A.T. Amos and G.G. Hall, Proc. R. Soc. A 263, 483 (1961).
9. R.L. Martin and E.R. Davidson, Phys. Rev. A. 16, 1341 (1977).
10. R.S. Mulliken, J. Chem. Phys. 23, 1833 (1955); 23, 1841 (1955); 23, 2338 (1955); 23, 2343 (1955).
11. P.S. Bagus, C.J. Nelin and B.O. Roos (to be published).
12. P.S. Bagus, C.J. Nelin, C.R. Brundle, and M. Seel (to be published).
13. D. Schmeisser, P. Avoaries, and J. Demuth (to be published).
14. T.C. Chiang, G. Kaindl, and D.E. Eastman, Solid State Commun. 36, 25 (1980).
15. K.P. Huber and G. Herzberg, Constants of Diatomic Molecules, (Van Nostrand, New York, 1979).
16. C.W. Bauschlicher, Jr., C.J. Nelin and P.S. Bagus (to be published).
17. Y. Lefebvre, B. Pinchemel, J.M. Delaval and J. Schamps, Phys. Scripta 25, 329 (1982).
18. J.N. Allison and W.A. Goddard III, J. Chem. Phys. 77, 4259 (1982).
19. C.E. Moore, Atomic Energy Levels, Natl. Bur. Stand. (U.S.), cir. 467 (1949). All energies are given as the weighted average over  $M_j$  values.

20. A.J.N. Wachters, J. Chem. Phys. 52, 1033 (1970).
21. P.J. Hay, J. Chem. Phys. 66, 4377 (1970).
22. T.H. Dunning, Jr., J. Chem. Phys. 53, 2823 (1970).
23. B.O. Roos, P.R. Taylor and P.E.M. Siegbahn, Chem. Phys. 48, 157 (1980).

TABLE I

Comparison between the population analyses obtained for an SCF calculation of an  $\text{Al}_4(1,3)\text{CO}$  cluster, (111) face, using four all electron Al atoms and using one all electron Al atom with three ECP Al atoms (3 electron). The calculations have  $C_{3v}$  symmetry; the Al-CO distance is 1.98Å, the Al lattice spacing is 4.05Å, and the C-O distance is 1.15Å. The state compared is  $^3A_2$  with valence occupation  $a^2e^2$ . Also included is a comparison of the results for an optimize Al-CO distance.

<u>Top Al Atom</u>	<u>4 All Electron</u>	<u>1 All Electron</u>
3s	1.31	1.28
total $3p_x 3p_y$	1.40	1.41
$3p_z$	0.56	0.51
Q	-0.27	-0.21
<u>Adsorbed CO</u>		
$\sigma$ population	-0.15	-0.15
$\pi$ population	+0.40	+0.35
Q	-0.25	-0.20
<u>Properties for</u>		
<u>Optimize CO-Al</u>		
$r_{\min}(\text{CO-Al})$	1.98Å	2.00Å
$D_e$	0.23eV	0.23eV



TABLE II

Comparison between the results for an SCF calculation of a  $\text{Ni}_5(1,4)\text{CO}$  cluster, (100) face, using a) 5 all electron Ni atoms, b) 1 all electron Ni atom with 4 ECP Ni atoms (1 electron), and c) 5 ECP Ni atoms (1 electron). The Ni lattice spacing is 3.52Å; the Ni-CO distance is held fixed at 1.84Å, and the C-O distance is 1.15Å.

	<u>5 All Electron</u>	<u>1 All Electron 4ECP</u>	<u>5 ECP</u>
$\Delta E$	0.46eV	0.54eV	1.33eV
$\text{CO}(\sigma)$	-0.15	-0.15	-0.15
$\text{CO}(\pi)$	+0.19	+0.16	+0.03

TABLE III

Summary of calculations for Cr atom and  $\text{Cr}^+$  ion and for Mo atom and  $\text{Mo}^+$  ion. Separation,  $\Delta$ , is in  $\text{cm}^{-1}$  and the total energy is in Hartrees.

	Cr			$\text{Cr}^+$		
	$E(3d^5 4s^1)$	$E(3d^4 4s^2)$	$\Delta$	$E(3d^5)$	$E(3d^4 4s^1)$	$\Delta$
SCF	-1043.2636	-1043.2175	10,120	-1043.0465	-1043.0046	9,200
SDCI	-1043.3221	-1043.2866	7,790	-1043.0950	-1043.0351	13,150
EXP <sup>a</sup>			8,090			12,280

	Mo			$\text{Mo}^+$		
	$E(4d^5 5s^1)$	$E(4d^4 5s^2)$	$\Delta$	$E(4d^5)$	$E(4d^4 5s^1)$	$\Delta$
SCF	-3975.4551	-3975.3487	23,350	-3975.2385	-3975.1557	18,170
SDCI	-3975.5268	-3975.4414	18,440	-3975.2948	-3975.2600	7,640
EXP <sup>a</sup>			11,830			12,800

<sup>a</sup> Ref. 18.

TABLE IV

The CAS (MCSCF) and SDCI results for the lowest  $5\Pi$  and  $5\Sigma^+$  states of CrO. The properties given are the equilibrium Cr-O bond distance,  $r_e$ , the vibrational frequency,  $\omega_e$ , and the dissociation energy  $D_e$ . Also given are the energetic separation of the states,  $\Delta$  and the correlation energy obtained for the SDCI wavefunction. These last two properties are computed at  $R = 1.615\text{\AA}$ .

		$5\Pi$	$5\Sigma^+$	$\Delta(\text{cm}^{-1})$
SCF	$r_e^{\circ}(\text{\AA})$	1.86	1.86	
	$\omega_e(\text{cm}^{-1})$	630	420	
	$D_e(\text{eV})$	2.52	1.34	7210
SDCI	$r_e$	1.66	1.68	
	$\omega_e$	820	750	
	$D_e$	2.82	2.33	5375
	$E_{\text{corr}}(\text{eV})$	6.82	7.05	
Exp. <sup>a</sup>	$r_e$	1.615		
	$\omega_e$	898.4		

<sup>a</sup> See ref. 15.

TABLE V

The CAS (MCSCF) and CI results for the lowest  $5\Pi$  and  $5\Sigma^+$  states of MoO. The properties given are the equilibrium Mo-O bond distance,  $r_e$ , the vibrational frequency,  $\omega_e$ , the dissociation energy,  $D_e$ . Also given are the energetic separation of the states,  $\Delta$  and the correlation energy obtained for the SDCI wavefunction. These last two properties are computed at  $r = 1.77\text{\AA}$ .

		$5\Pi$	$5\Sigma^+$	$\Delta$
SCF	$r_e$ (Å)	1.80	1.82	
	$\omega_e$ (cm <sup>-1</sup> )	560	730	
	$D_e$ (eV)	2.13	1.41	6040
SDCI	$r_e$	1.71	1.77	
	$\omega_e$	1035	830	
	$D_e$	3.54	2.63	
	$E_{\text{corr}}$ (eV)	7.29	7.25	6350
Exp. <sup>a</sup>	$r_e$	--	--	
	$\omega_e$	--	--	
	$D_e$	5.0eV	--	

<sup>a</sup> See ref. 15.

TABLE VI

The resulting CAS and SDCI d population, the net charge on the Cr atom and the net overlap population for the four computed states of CrO at  $r = 3.452$  a.u.

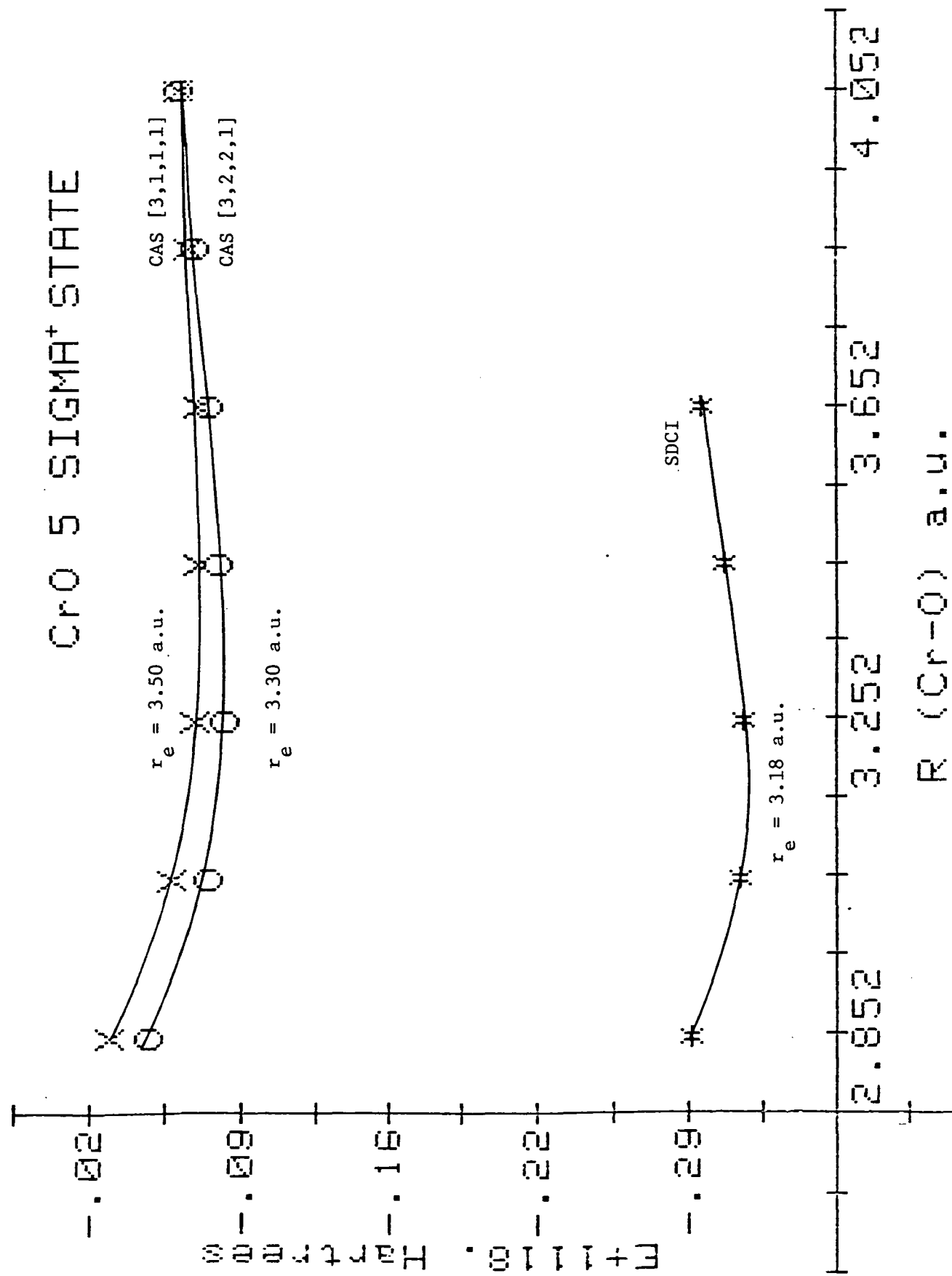
	$5_{\Pi}$	$5_{\Sigma^+}$	$7_{\Pi}$	$7_{\Sigma^+}$
CASSCF				
d	4.26	4.98	4.25	4.23
Q	0.63	0.81	0.64	0.68
overlap	0.33	0.30	0.25	--
SDCI				
d	4.35	4.89	4.35	4.32
Q	0.53	0.78	0.53	0.58
overlap	0.46	0.52	0.32	0.34

TABLE VII

The resulting CAS and SDCI 4d population, the net charge on the Mo atom and the net overlap population for the four computed states of MoO.

		$5_{\Pi}$	$5_{\Sigma^+}$	$7_{\Pi}$	$7_{\Sigma^+}$
<hr/>					
r(Mo-O) (a.u.)		3.35	3.35	3.95	3.95
CASSCF					
	d	4.47	4.89	4.69	4.80
	Q	0.59	0.82	0.64	0.74
	overlap	0.42	0.32	0.24	0.18
SDCI					
	d	4.47	4.90	4.73	4.84
	Q	0.53	0.73	0.54	0.64
	overlap	0.54	0.43	0.30	0.26

Figure 1



ORIGINAL PAGE IS  
OF POOR QUALITY

Figure 2

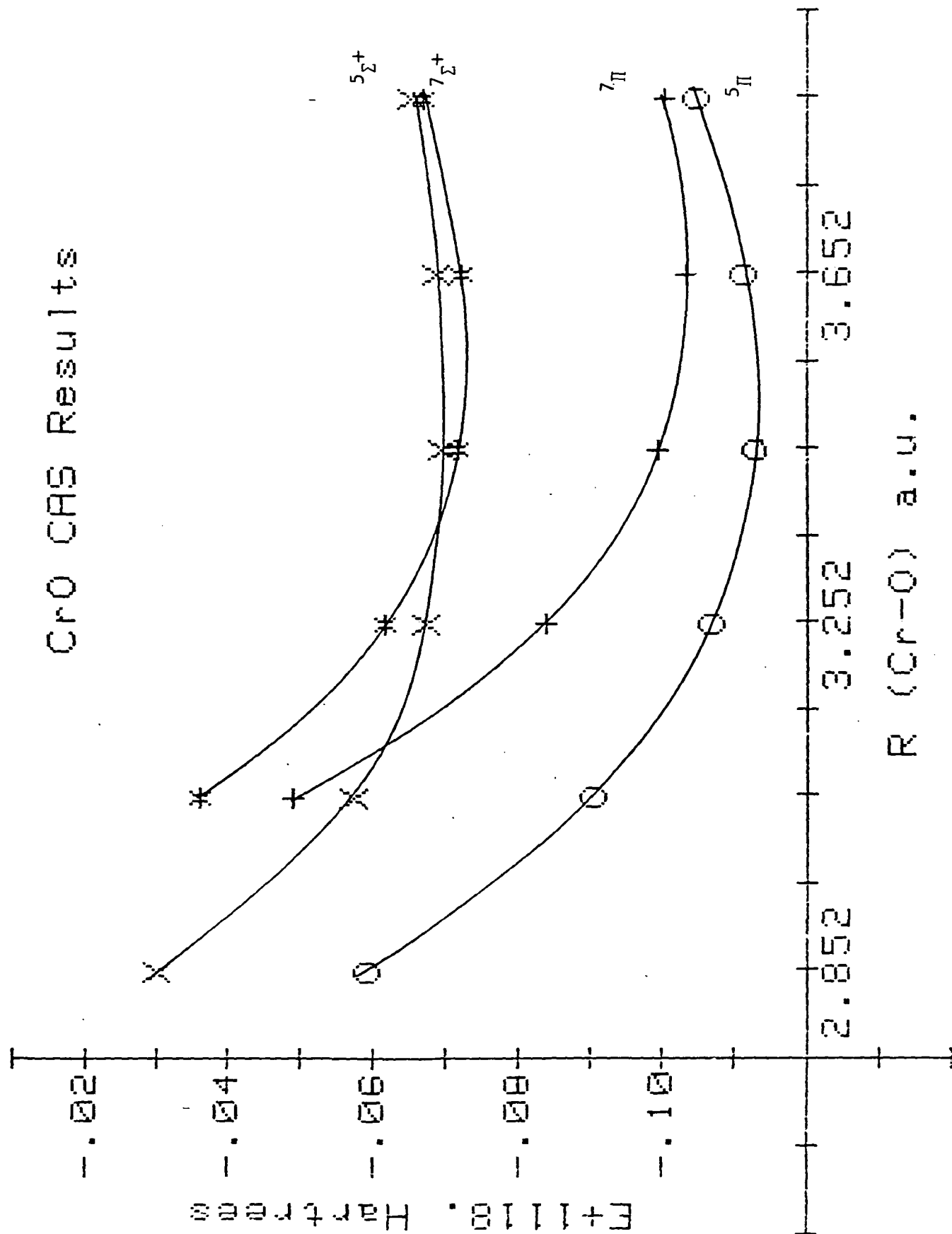




Figure 3

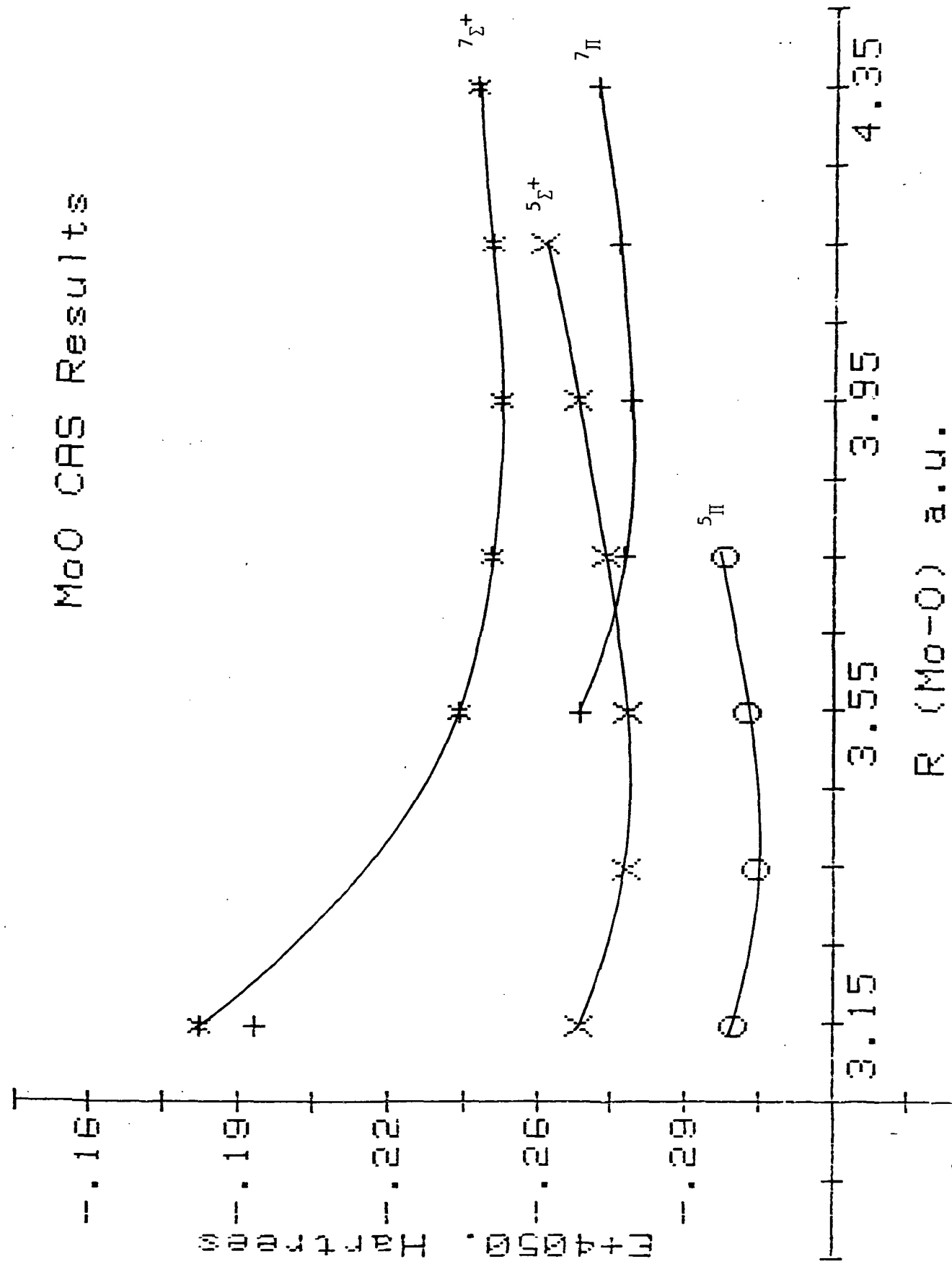


Figure 4

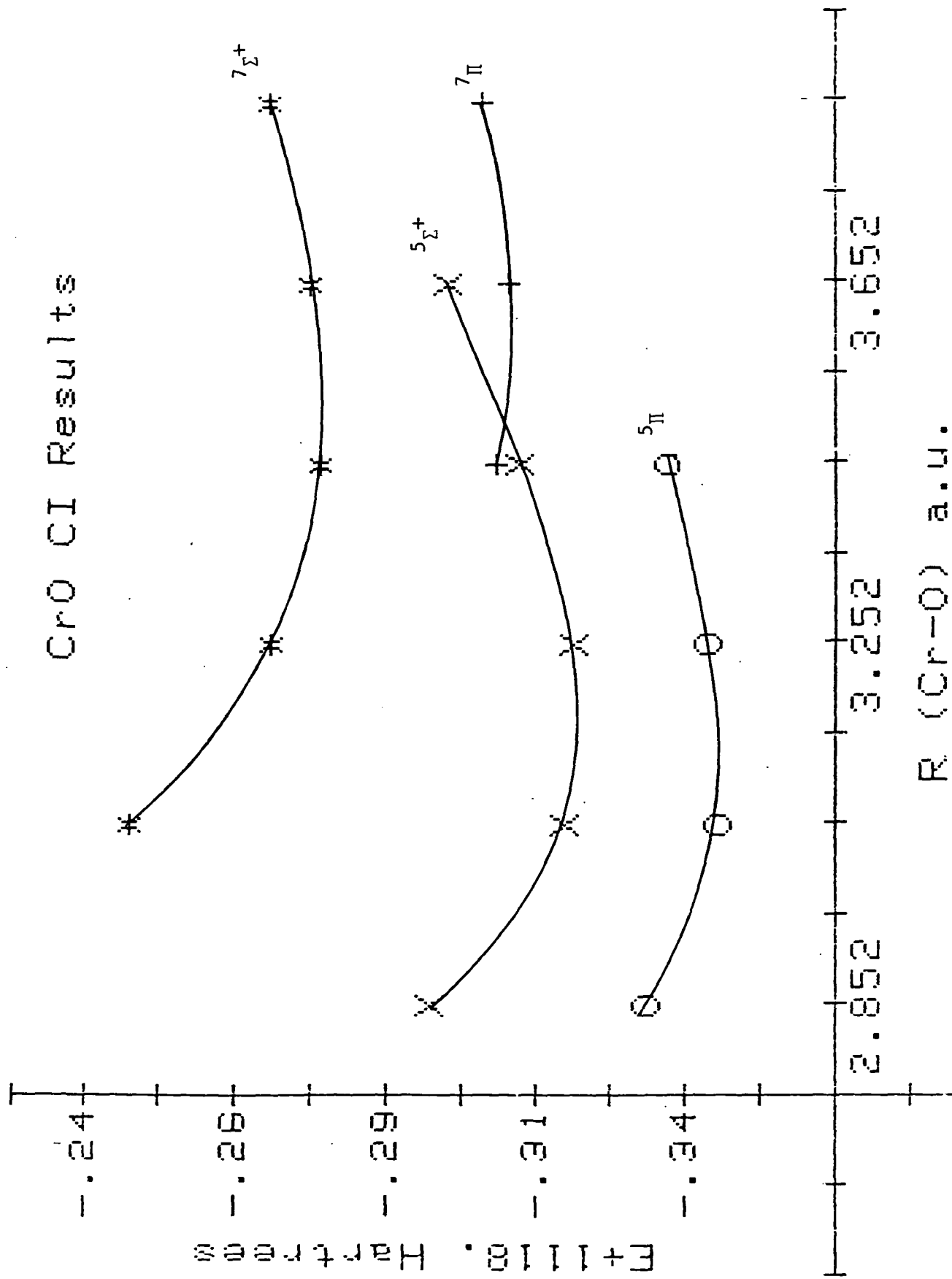
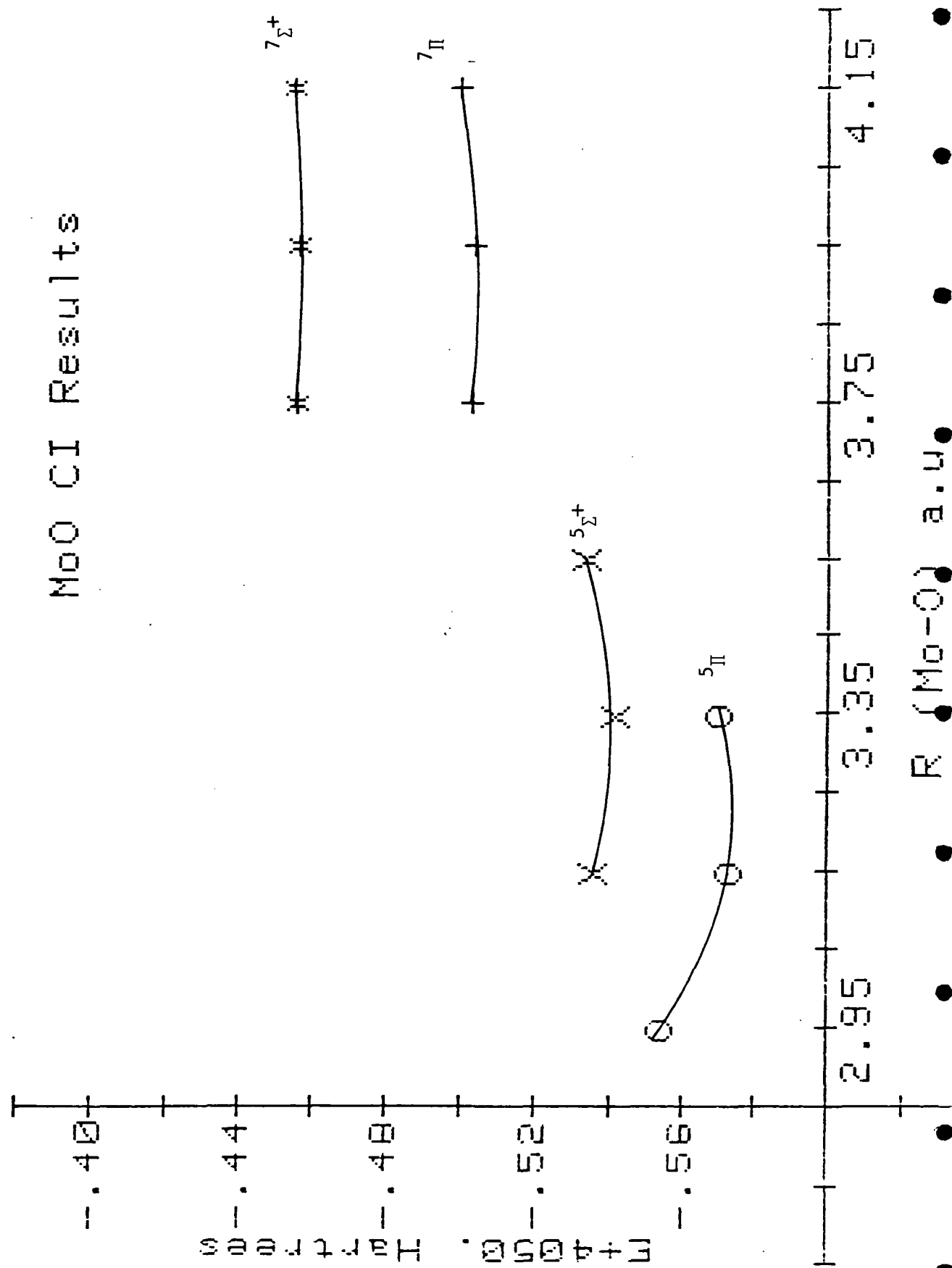


Figure 5

# MoO CI Results



## CHARGING AND HYBRIDIZATION IN THE FINITE CLUSTER MODEL

Charles W. Bauschlicher, Jr.

(accepted Chemical Physics Letters)

NASA Ames Research Center  
Moffett Field, California 94035

Paul S. Bagus

IBM Research Laboratory  
San Jose, California 95193

Constance J. Nelin

Polyatomics Research Institute  
Mountain View, California 94043

N86-29927

18317

**ABSTRACT:** Cluster wavefunctions which have appropriate hybridization and polarization lead to reasonable properties for the interaction of an adsorbate with a solid surface. However, for Al clusters, we find that the atomic charge distribution is not uniform. The finite cluster size leads to charges not representative for an extended system. This effect appears to be dependent on the particular material being studied; it does not occur in all cases.

\*Mailing address: 1101 San Antonio Road, Suite 420.

The success of the cluster model to investigate some chemisorption problems relies on the local nature of the bonding of the adsorbate and metal surface atoms. Therefore, one must have a cluster large enough that all the atoms used to simulate an adsorption site on a metal surface have the same charge and hybridization and that these properties must be similar to that in the actual metal surface. We have investigated the question of the convergence of the cluster model for the chemisorption of H on a Be(1000) surface with respect to the cluster size.<sup>1,2</sup> We have considered clusters as large as Be<sub>36</sub>(14,8,14) (where the notation Be<sub>k</sub>(n,ℓ,m) indicates n atoms in the first layer, ℓ in the second and m in the third) and have concluded, that while the dissociation energy of the H from the surface, D<sub>e</sub>, converges very slowly with cluster size, properties such as the height above the surface, r<sub>e</sub>, the vibrational frequency normal to the surface, ω<sub>e</sub>, and the nature of the bonding converge more rapidly. Our rule of thumb was that when all the atoms involved in the bonding have all their nearest neighbors, r<sub>e</sub>, ω<sub>e</sub> and the nature of the bonding are effectively converged. We have shown that the number of neighbors is very important in determining the hybridization of the Be and Mg atoms,<sup>3</sup> clearly a sufficient number of neighbors must be present so that the hybridization of the bonding atoms is similar to an atom in a metal surface. The cluster results support the view that the first nearest neighbors are needed for local properties to be converged. A simple example of this is H on Be(1000) at a three-fold site when there is no atom in the second layer below the incoming H atom; this is called the open site. Summarized in Table I are the r<sub>e</sub>, ω<sub>e</sub> and the atomic populations for the Be atoms directly involved in the H bonding at the open site for various size Be clusters. The results given are for minimal basis set SCF calculations. The smallest cluster, Be<sub>3</sub>(3,0), includes only the directly bonding open site Be atoms. The largest cluster, Be<sub>36</sub>, includes both first and second-nearest neighbors of these bonding Be atoms in the first three layers of the surface. The clusters and computational approach are described in detail elsewhere.<sup>1,2</sup> For

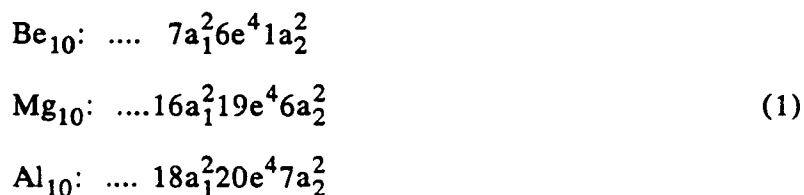
all but  $\text{Be}_{22}$  and  $\text{Be}_{36}$ , the bonding Be atoms are equivalent in the  $C_{3v}$  symmetry of the clusters. For  $\text{Be}_{22}$  and  $\text{Be}_{36}$ , the cluster has only  $C_s$  symmetry and the average values of the populations for the nearly equivalent bonding atoms are given in Table I. The atomic valence electron population is decomposed into its 2s and 2p character.

The variation of the computed  $\omega_e$  is small among the various clusters. However, there are considerable changes in the  $r_e$ . These changes can be related to the hybridization and, in particular, the decomposition of the p character into  $p_z$ , normal to the surface plane, and  $p_x$  or  $p_y$ , in the plane. The directional character of the p orbital allows the formation of strong bonds and correspondingly short bond lengths. However, there is competition for use of the  $p_z$  electrons to bond to the adsorbed H and to bond the first to the second layer of the cluster.<sup>1</sup> The H atom can also bond with the  $p_x$  and  $p_y$  Be electrons. However, this can only occur when the H atom approaches more closely to the surface. These two effects are the reason for the dramatic reduction in  $r_e$  when a second plane is added to the cluster; note  $r_e$  for  $\text{Be}_6(6,0)$  and  $\text{Be}_4(6,3)$ . It is not surprising that one needs neighbors both in the surface plane and in the lower planes to induce the correct hybridization in the bonding atoms and to correctly represent the formation of metal-metal bonds.

We have also investigated the chemisorption of oxygen on  $\text{Al}(111)$ .<sup>4,5</sup> For the bare  $\text{Al}_{19}$  cluster we found a charge of  $-0.29$  electrons on the three central Al's.<sup>4</sup> For this system, the oxygen-Al interaction is strong and O is negative because of a transfer of charge from the Al atoms. Thus, the charge buildup at the central, bonding, atoms was assumed to only slightly effect the results; this is supported by the reasonably accurate results for  $r_e$ . However, for weaker interactions, such charging of the bonding atoms might lead to serious errors. In this letter, we report on variations in charge distribution for several small clusters. Minimum basis sets were used throughout this work in large part because of the model nature

of the calculations. The Be minimum basis is a 3 Gaussian type orbital (GTO) fit to 1s, 2s and 2p Slater type orbitals (STO). This basis set is the same as that used previously and has been denoted Minimum basis IIb.<sup>1,2</sup> Both the Al and Mg basis sets are (633(s),42(p)) contractions of the Roos and Siegbahn (10s6p) primitive set<sup>6</sup> for Al and their (10s4p) Mg basis with two p functions added to represent the 3p orbital.<sup>7</sup> Symmetry and equivalence restricted SCF calculations were performed. The metal structure and metal-metal distances are taken from the bulk values.<sup>8</sup> The Molecule-Alchemy program system<sup>9</sup> was used throughout this work.

Be and Mg form hcp crystals and Al has fcc structure. For chemisorption at a directly overhead site on either the (111) surface of an fcc crystal or the (1000) surface of an hcp crystal, a 10 atom 2 layer cluster would appear to be appropriate. The central metal atom, the adsorption site, has its 6 nearest neighbors in the surface plane and its 3 nearest second layer neighbors. This  $X_{10}(7,3)$  cluster is shown in Figure 1. The total populations of the three distinct cluster atoms – central, first layer edge and second layer – are reported in Table II for  $Be_{10}$ ,  $Mg_{10}$  and  $Al_{10}$ . The  $C_{3v}$  closed shell configurations used are:



For  $Be_{10}$  and  $Mg_{10}$ , the charges on the three types of atoms are essentially the same and essentially neutral. This is not true for  $Al_{10}$  where the central atom is negatively charged by 0.63 electrons. The gross atomic populations may be misleading because of the arbitrary assignment of overlap populations to atoms. However, the different behavior for Al from Mg and Be strongly suggests that the central Al is indeed negatively charged. In order to further test the population analysis results, we examined the 1s orbital energies; these are also shown

in Table II. Although the orbital energies are influenced by the detailed distribution of charge in the cluster, they should reflect the effective charges on the atoms. They are a measure, through Koopman's theorem, of the ionization potential, IP. The 1s IP for a negatively charged atom is smaller than that for a neutral or positive one. The changes among the  $\epsilon_{1s}$ 's shown in Table II are consistent with the differences in the Mulliken population analysis charges. In particular, the central atom  $\epsilon_{1s}$  in  $\text{Al}_{10}$  is larger (less negative) than the edge atom  $\epsilon_{1s}$ 's. For  $\text{Mg}_{10}$  and  $\text{Al}_{10}$ , we also examined the wavefunctions for states very close in energy to those of Eq. (1). The behavior of the populations and the  $\epsilon_{1s}$ 's is similar to that shown in Table II. All our results lead to the central atom in  $\text{Al}_{10}$  being significantly negatively charged while in  $\text{Mg}_{10}$  or  $\text{Be}_{10}$  it is essentially neutral.

We also examined 13 atom clusters designed to simulate the bulk environment for a central atom by surrounding it with its 12 nearest neighbors. For the hcp systems, Be and Mg, the cluster was  $\text{X}_{13}(3,7,3)$  and we obtained SCF solutions for the lowest  $\text{D}_{3h}$  closed shell state. For fcc Al, the cluster was  $\text{X}_{13}(4,5,4)$  and the SCF solution was for the lowest doublet state with a single open shell in  $\text{O}_h$  symmetry. As for  $\text{X}_{10}$ , the z axis is defined normal to the cluster layer. The valence level populations of the central atom for these  $\text{X}_{13}$  systems is given in Table III where the populations are divided into s,  $p_x + p_y$  and  $p_z$  character. The symmetry of the clusters is such that  $p_x \equiv p_y$ . The  $\text{X}_{13}$  populations are compared to those for the  $\text{X}_{10}$  clusters. As in the case of the two-layer cluster, the central Al has a far larger charge than do the Be or Mg central atoms; in  $\text{Al}_{13}(3,7,3)$ , it is essentially  $\text{Al}^-$ . For Be and Mg, increasing the number of neighbors also increases the charge on the central atom, but by much less than in the case of Al.



The effect of the addition to the cluster of the atoms which are second nearest neighbors of the central atom is also of interest. However, this would lead to rather large clusters if we extend the  $X_{10}$  or  $X_{13}$  systems. Therefore, we chose to investigate this effect with clusters containing only one layer of atoms. For Be, we considered only  $Be_7$  containing the nearest neighbors of a central atom on the (1000) face. For Al, we considered the (100) face and used  $Al_5$  and  $Al_{13}$  clusters. The  $Al_5$  cluster contains a central atom and its four nearest neighbors; for  $Al_{13}$ , we added the 8 second nearest neighbors of the central atom to  $Al_5$ . We obtained SCF solutions for the lowest closed shell configuration for  $Be_7$  and for the lowest single open shell configurations for  $Al_5$  and  $Al_{13}$ . The central atom populations for these clusters are also given in Table III.

Compared to the  $X_{13}$  populations, the charge on the central atom in  $Al_5$  is reduced by 0.21 electrons; in  $Be_7$ , it is reduced by 0.11 electrons. The central Al atom in  $Al_5$  is still significantly negative while all the atoms, central and edge, in  $Be_7$  are nearly neutral. The most interesting result comes when we consider the central atom charge in  $Al_{13}$  which contains both first and second nearest neighbors. The charge is reduced by 0.69 electrons from that in  $Al_5$ ; the central atom is now nearly neutral! The central atom in  $Al_{13}$  has virtually no overlap population with the modestly distant second nearest neighbors. Moreover, the overlap population between the central atom and its nearest neighbors is almost the same for  $Al_5$  and  $Al_{13}$ . Hence, clearly, the electron distribution about the central atom has changed dramatically when its second nearest neighbors are added to the cluster. The change in the population analysis charge from  $-0.78e$  in  $Al_5$  to  $-0.09e$  in  $Al_{13}$  is not a consequence of artifacts in the analysis. There is also a large change in the charge distribution for the central atom's nearest neighbors between  $Al_5$  and  $Al_{13}$ . They were positively charged 0.20 in the small cluster and are negatively charged by 0.37 electrons in

$\text{Al}_{13}$ . The entire view of how bonding would take place could be altered by changes of this magnitude.

As for  $\text{Al}_{10}(7,3)$ , we found two low-lying states for  $\text{Al}_{13}(13,0)$ . For  $\text{Al}_{13}$ , unlike the results for  $\text{Al}_{10}$ , the charge distributions for the two states are fairly different. The central Al atom is more nearly neutral for both  $\text{Al}_{13}$  states than it was for  $\text{Al}_5$ . However, the second state, higher in energy than that discussed above by only 0.04 eV, has a charge on the central Al atom of 13.31. Thus, the addition of second nearest neighbors is not sufficient to insure that all the low lying states have a near neutral central atom. We conclude that in addition to the total energy of various states, the charge on the metal atoms directly involved in forming the chemisorption bond should also be used as a criterion for choosing the state to be used in studying adsorption. For the simulation of a metal surface, these atoms should be nearly neutral.

Another interesting question concerns the extent of the hybridization of the central, adsorption site, atoms in the clusters. It is known, for example, that in many Al compounds, a 3s electron is promoted to 3p leading to trivalent Al. We find that the central atom in the three-dimensional  $\text{Al}_{13}(4,5,4)$  cluster has a 3s population of 1.12e (see Table III) consistent with a trivalent atom. We find similar central atom hybridization for the two layer  $\text{Al}_{10}(7,3)$  and both the one layer clusters,  $\text{Al}_5(5,0)$  and  $\text{Al}_{13}(13,0)$ . It would appear that the first nearest neighbors are sufficient to lead to a substantial 3s to 3p promotion. Previously,<sup>3</sup> we observed that there was a very large change in the Mg hybridization, as measured by the number of 3p electrons, between tetrahedral  $\text{Mg}_4$ , 0.22, and  $\text{Mg}_{13}(3,7,3)$ , 0.85. We note that in  $\text{Mg}_{10}(7,3)$  the total 3p population is 0.54e; less than  $\text{Mg}_{13}(3,7,3)$  but considerably larger than tetrahedral  $\text{Mg}_4$ . The ns to np promotion for the central atom in  $\text{Al}_{10}$  and  $\text{Be}_{10}$

is also less than for  $\text{Al}_{13}(4,5,4)$  or  $\text{Be}_{13}(3,7,3)$ , respectively. However, in all three cases there is substantial s to p promotion for the central atom of the  $\text{X}_{10}$  clusters.

Ideally one would like to use a cluster sufficiently large so that all problems of charging and hybridization arising from its finite size are eliminated; this is not always possible and one must find the correct balance between computer time, finite cluster effects and the accuracy needed to resolve the problem. In the past we have found it quite useful to use small clusters for the preliminary calculations, thus reducing the number of expensive large cluster calculations. The question naturally arises whether the results obtained with small clusters are meaningful. The answer depends, at least in part, on the strength of the interaction and the quality of the information desired. For weak interactions, charge buildup of the magnitude found for  $\text{Al}_{10}$  may lead to seriously questionable results; for very strong interactions, it might add some uncertainty but useful information might still be gained. It would also appear reasonable to investigate initially a large bare cluster. Then to proceed with smaller clusters which have a similar charge distribution as the large cluster for the atoms which will be directly involved in bonding to an adsorbate. Preliminary results appear to support this view. Also, our recent work shows that sometimes the charge distribution for excited states of the smaller clusters are closer to that of the large cluster than is that for the small cluster ground state. Thus, it may be appropriate to use these excited states for the study of chemisorption. In this way, it should very often be possible to find a small cluster with reasonable charge distributions. However, it should be cautioned that there may be problems associated with performing SCF calculations on excited states if the addition of the adsorbate lowers the point group symmetry of the cluster.

Our previous work for the chemisorption of H/Be(1000) provides guides for the size of a cluster needed to reduce the artifacts, or errors, associated with using a finite cluster to

model a semi-infinite surface. However, it is clear that the magnitude of finite cluster effects varies from material to material and is even different for different faces of a crystal.

Therefore, the question of the appropriate cluster size must be investigated separately for each chemisorption problem.

Table I. Summary of the height of H above the surface,  $r_e$  in Å, vibrational frequency for motion normal to the surface,  $\omega_e$  in  $\text{cm}^{-1}$ , and adsorption site Be atom populations for H/Be(1000) at the open site. The Be populations are given for one of the three equivalent adsorption site atoms. They are divided into 2s,  $2p_x$ ,  $2p_y$ ,  $2p_z$  and  $2p=2p_x+2p_y+2p_z$  character. The cluster surface is taken as the xy plane.

Cluster	2s	$2p_x+2p_y$	$2p_z$	2p	$r_e$	$\omega_e$
Be <sub>3</sub> (3,0)	1.18	0.45	0.34	0.79	1.21	1230
Be <sub>6</sub> (6,0)	0.85	0.86	0.38	1.24	1.12	1150
Be <sub>6</sub> (3,3)	0.76	0.83	0.41	1.25	1.05	1200
Be <sub>9</sub> (6,3)	0.77	0.78	0.52	1.30	1.05	1160
Be <sub>22</sub> (14,8)	0.62	--	--	1.41	0.94	1230
Be <sub>36</sub> (14,8,14)	0.54	1.05	0.42	1.48	0.90	1200

Table II. Atomic charges and 1s orbital energies,  $\epsilon_{1s}$  in hartrees, for the  $X_{10}(7,3)$  clusters for Be, Mg and Al. Results are given for the three distinct types of atoms; central, first layer edge and second layer.

Atom Type	Be		Mg		Al	
	Charge	$\epsilon_{1s}$	Charge	$\epsilon_{1s}$	Charge	$\epsilon_{1s}$
Central	3.93	-4.6203	11.91	-49.0656	13.63	-58.1445
Edge	3.98	-4.6108	12.00	-49.0695	12.90	-58.2005
Second Layer	4.07	-4.5847	12.02	-49.0366	12.99	-58.2085

Table III. Central atom populations for one layer and two layer surface clusters and for three layer bulk clusters for Be, Mg and Al. The total population is divided into s,  $p_x$ ,  $p_y$  and  $p_z$  character. The xy plane is the taken as the plane of the layers of the clusters.

		Three Layer $X_{13}$	Two Layer $X_{10}$	One Layer Clusters	
				First Neighbors	Second Neighbors
Be	{ total	4.09	3.93	3.98	----
	{ 2s	0.65	0.79	0.42	----
	{ $2p_z$	0.82	0.34	0.86	----
	{ $2p_x+2p_y$	0.62	0.80	0.70	----
Mg	{ total	12.11	11.91	----	----
	{ 3s	1.23	1.36	----	----
	{ $3p_z$	0.33	0.12	----	----
	{ $3p_x+3p_y$	0.50	0.42	----	----
Al	{ total	13.99	13.63	13.78	13.09
	{ 3s	1.12	1.21	1.29	1.29
	{ $3p_z$	0.92	0.70	0.62	0.37
	{ $3p_x+3p_y$	1.84	1.70	1.88	1.42

## REFERENCES

1. C. W. Bauschlicher, P. S. Bagus and H. F. Schaefer, *IBM J. Res. Develop.* 22, 213 (1978).
2. P. S. Bagus, H. F. Schaefer and C. W. Bauschlicher, *J. Chem. Phys.*, in press.
3. C. W. Bauschlicher, P. S. Bagus and B. N. Cox, *J. Chem. Phys.* 77, 4032 (1982).
4. B. N. Cox and C. W. Bauschlicher, *Surf. Sci.* 115, 15 (1982).
5. P. S. Bagus, I. P. Batra, C. W. Bauschlicher and R. Broer, *J. Elec. Spec.*, in press.
6. B. Roos and P. E. M. Siegbahn, *Theo. Chim. Acta.* 17, 209 (1970).
7. A. D. McLean and G. S. Chandler, *J. Chem. Phys.* 72, 5639 (1980).
8. J. Donohue, "The Structure of the Elements," Wiley Interscience Publishers, New York, 1974.
9. The MOLECULE-ALCHEMY program package incorporates the MOLECULE integrals program written by J. Almlöf and the ALCHEMY SCF program written by P. S. Bagus and B. Liu. The interfacing of the programs was performed by U. Wahlgren and P. S. Bagus.



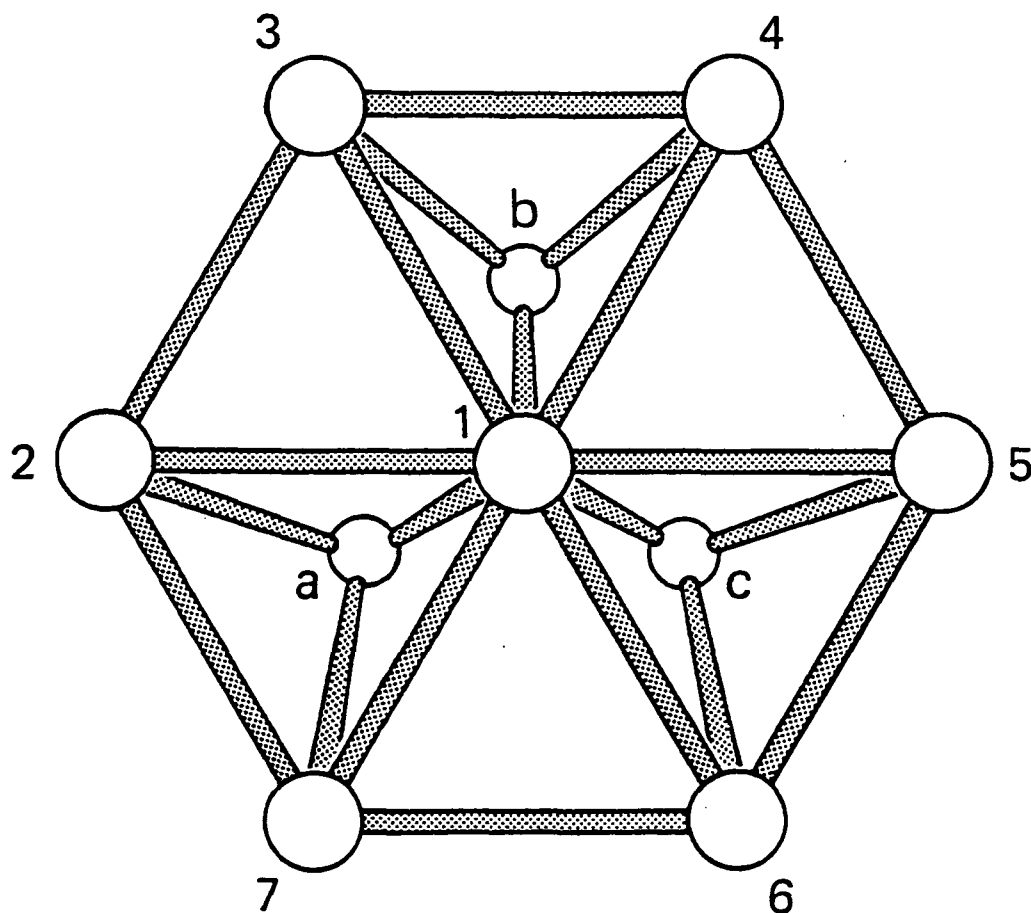


**Figure 1.** Geometry of the two layer  $X_{10}(7,3)$  clusters. The central, absorption site, atom is number 1; the first layer edge atoms are numbered 2 through 7; and the second layer atoms are lettered a through c.

D4-25

208

N86-29928

## ON THE LOW-LYING STATES OF CuO

Paul S. Bagus

(accepted Journal of Chemical Physics)

IBM Research Laboratory  
San Jose, California 95193

- 1A 056249

18318

Constance J. Nelin\*

University of Lund  
Lund, Sweden

= 9318811

Charles W. Bauschlicher, Jr.\*\*

Polyatomic Research Institute  
Mountain View, California 94043

- PY 097681

**ABSTRACT:** Self-consistent-field and correlated wave functions have been computed for the ground and for several low-lying states of CuO. The ground state is  $X^2\Pi$  and the lowest excited state, at  $\sim 8,000\text{ cm}^{-1}$  above  $X^2\Pi$ , is a previously unidentified  $^2\Sigma^+$  state. The separation of these states is compared to that for the similar states of KO and is analysed in terms of integrals between orbitals of the separated free ions. We consider a classification of the states of the molecule based on states of  $\text{Cu}^+$  and  $\text{O}^-$  which leads to a division into manifolds of states arising from  $\text{Cu}^+ 3d^{10}$  and  $\text{Cu}^+ 3d^9 4s^1$ . We predict that the states of the  $3d^9 4s^1$  manifold are  $10,000\text{--}30,000\text{ cm}^{-1}$  above the ground state and assign the observed  $A^2\Sigma^+$  state at  $16,500\text{ cm}^{-1}$  to this manifold.

\*Present address: Polyatomics Research Institute, 1101 San Antonio Road, Suite 420, Mountain View, California 94043.

\*\*Present address: NASA Ames Research Center, Moffett Field, California 94035.

## INTRODUCTION

As a preliminary step for the study of the chemisorption of oxygen on copper, we have investigated the bonding in the diatomic molecule CuO for both the ground and the low lying excited states. We find that the two lowest states are ionic and arise from  $\text{Cu}^+$  in a  $3d^{10}$  configuration; these are the  $X^2\Pi$  ground state and a previously unidentified  $A^2\Sigma^+$  state. We have also investigated additional ionic states which arise from  $\text{Cu}^+$  in a  $3d^9 4s^1$  configuration. We conclude that the state which had been identified<sup>1</sup> as the first excited state at  $T_e = 16,491 \text{ cm}^{-1}$  is likely to arise in this way. The separation between the  $X^2\Pi$  and  $A^2\Sigma^+$  states is much larger for CuO,  $\sim 8,000 \text{ cm}^{-1}$ , than for the similar ionic molecule  $\text{KO}^{1,2}$  where it is only  $\sim 350 \text{ cm}^{-1}$ . This difference is analysed in terms of the overlap and nuclear attraction integrals between the anion and cation atomic orbitals.

We consider a classification of states for CuO based on the properties of the separated atoms. The Cu atom has a  $2S(3d^{10} 4s^1)$  ground state; the first excited state,<sup>3</sup>  $3D(3d^9 4s^1)$ , is at  $12,019 \text{ cm}^{-1}$ . For  $\text{Cu}^+$ , the lowest state is  $1S(3d^{10})$  and the first excited state is  $3D(3d^9 4s^1)$  at  $22,648 \text{ cm}^{-1}$ . One expects CuO to be a very ionic molecule with essentially  $\text{Cu}^+$  and  $\text{O}^-$  character. The  $\text{O}^-$  anion can, in  $C_{\infty v}$  symmetry, be formed in two ways:  $\sigma^1 \pi^4$  ( $\sigma$  hole) or  $\sigma^2 \pi^3$  ( $\pi$  hole). When  $\text{O}^-$  is combined with  $\text{Cu}^+$ ,  $1S(3d^{10})$ , a  $2\Pi$  and a  $2\Sigma^+$  state can be formed. This is similar to the behavior found for the alkali monoxides,<sup>2,4</sup> LiO to CsO. We refer to these low-lying states as forming a manifold arising from  $3d^{10}$ .

If  $\text{O}^-$  is combined with the  $\text{Cu}^+$  in the  $3d^9 4s^1$  excited configuration a large number of states can arise. These states can be either ionic or mixed (ionic and covalent) in character. For the first type, those with essentially only ionic character, three  $\Pi$ , two  $\Sigma^+$ , two  $\Delta$ , one  $\Sigma^-$  and one  $\Phi$  state come from the interaction of  $\text{O}^-$  having either a  $\sigma$  or a  $\pi$  hole in the 2p shell with  $\text{Cu}^+$  having either a  $\sigma$ ,  $\pi$  or  $\delta$  hole in the 3d shell. The spin coupling of these

states is doublet or quartet. We refer to this class of states as purely ionic states. We should note that the Mulliken population for either the SCF or the multi-configuration SCF (MCSCF) wavefunctions for these states shows a charge of  $\sim 0.7$  and an overlap charge of  $\sim 0.3$ . Thus, they are not purely ionic; however, we refer to them in this way to distinguish them from states which also have a covalent bond. This second type of states arises when a covalent bond is formed between the  $O^- 2p\sigma$  and  $Cu^+ 4s$ . This can lead to three states,  $^2\Sigma^+$ ,  $^2\Pi$ , or  $^2\Delta$ , depending on the location of the d hole in  $Cu^+ (3d^9 4s^1)$ . We call these mixed states since they have both a covalent  $\sigma$  bond and an ionic contribution coming from  $Cu^+ O^-$ . We refer to the solely ionic and mixed states as forming a manifold arising from  $3d^9 4s^1$  (for short, the  $3d^9 4s^1$  manifold.) Given the separation between the  $3d^{10}$  and  $3d^9 4s^1$  states of  $Cu^+$  and the  $3d^{10} 4s^1$  and  $3d^9 4s^2$  states of Cu, it is reasonable to expect the  $3d^9 4s^1$  manifold of CuO to lie between 10,000 to 20,000  $cm^{-1}$  above the ground state. It is useful to consider this manifold as being formed from three groups of states. The first group comprises the three mixed states. The second group is composed of the ionic states for which  $O^-$  has the configuration  $2p\sigma^2 2p\pi^3$  and the third group of states where  $O^-$  is  $2p\sigma^1 2p\pi^4$ . We will present results for representative states of CuO in each of these groups.

For the CuO states discussed above, we have obtained LCAO SCF, MCSCF and single and double excitation configuration interaction, SDCI, wavefunctions. The basis set integral and SCF calculations were carried out using the MOLECULE-ALCHEMY program system.<sup>5</sup> The MCSCF calculations were performed using the CASSCF methods and programs developed by Roos *et al.*<sup>6</sup> and the SDCI calculations using the graphical unitary group direct CI program developed and implemented by Siegbahn.<sup>7</sup>

The organization of the paper is as follows. The details of the Gaussian basis sets are presented in Section II. In Sections III and IV, we discuss the nature and separation of the

lowest,  $3d^{10}$  manifold,  $^2\Pi$  and  $^2\Sigma^+$  states. We analyse and explain the role of the d electrons for the separation based on the overlap and nuclear attraction one-electron integrals. In Section V, we consider the nature of the excited CuO states that arise from the  $3d^9 4s^1$  manifold.

## II. BASIS SET DETAILS

Wavefunctions for CuO and KO have been computed in a basis of contracted Gaussian type orbitals. For both Cu and K, we have used the exponents optimized by Wachters<sup>8</sup> including two functions which represent the 4p orbital. (Those for  $3d^{10} 4s^1$ ,  $^2S$  were used for Cu.) We have added a diffuse d function to this set. For Cu, we used the value determined by Hay<sup>9</sup> and for K, we chose the exponent  $\alpha=0.4$ . These basis functions were contracted slightly differently than recommended by Wachters<sup>8</sup> in order to have the largest flexibility for either ionic (cationic) or neutral character for the metal 3p orbital. The oxygen basis set is based on Dunning's<sup>10</sup> double zeta contraction of Huzinaga's primitive set to which we have added a diffuse p,  $\alpha=0.059$ , to represent the  $O^-$  character and a d,  $\alpha=0.90$ . These added exponents have values close to those given by Dunning and Hay.<sup>11</sup> The final basis sets are: Cu(14s11p6d/8s6p4d), K(14s11p1d/8s6p1d), and O(9s6p1d/4s3p1d).

## III. STATES ARISING FROM $3d^{10}$ MANIFOLD

Symmetry and equivalence restricted SCF calculations were performed for the  $X^2\Pi$  and the lowest  $^2\Sigma^+$  states. CI wavefunctions consisting of all single and double excitations (SDCI) from the SCF reference were also obtained for these states. The SDCI excitation level is defined for a  $C_{\infty v}$  reference state. Thus for the  $2p\pi^3 X^2\Pi$  state, configurations which involve certain excitations of three spin orbitals are also included. In these SDCI calculations, excitations were permitted for only 17 electrons. The lowest  $6\sigma$  and  $2\pi$  SCF orbitals were frozen. These orbitals correspond to the Ar core of Cu and to the O1s.

Excitations were not allowed into the highest five  $\sigma$  and two  $\pi$  virtual SCF orbitals. For our basis, these orbitals are clearly functions which would correlate the frozen cores.

The results of these calculations are summarized in Table I. The separation between the  $X^2\Pi$  and the  $A^2\Sigma^+$  states is only slightly changed by the inclusion of correlation. The change in the separation between the SCF and CI calculations is only 0.14 eV while the total correlation energy is  $\sim 10.8$  eV. The small change is consistent with the view of an ionic system with small interatomic (molecular) correlation. The computed separation of only  $\sim 8,000\text{ cm}^{-1}$  is very different from the reported value<sup>1</sup> of  $16,491\text{ cm}^{-1}$ . This leads us to conclude that the state previously identified as the  $A^2\Sigma^+$  state is not the first excited state. It is likely that it is a higher state arising from the  $3d^9 4s^1$  manifold, as we will discuss below.

The computed equilibrium bond distance,  $r_e$ , for the  $X^2\Pi$  state at the SCF level is much longer than the experimental value of  $1.72\text{\AA}$ . When correlation is included, the bond shortens. This is similar to other calculations on transition metal compounds,<sup>12-14</sup> where correlation also shortens the bond. Even at the SDCI level, the agreement with experiment is poorer than one might have expected. However, the well is very shallow (see the vibrational frequencies given in Table I), and thus small errors due to the basis set or level of correlation can result in large errors in  $r_e$ . Based on our calculated results, the experimentally unidentified  $^2\Sigma^+$  state will have an  $r_e$  which is the same or slightly shorter than that for the  $X^2\Pi$  state and a slightly lower vibrational frequency,  $\omega_e$ .

We further investigated the correlation effects on the bond length by performing a multi-reference SDCI calculation for the  $^2\Sigma^+$  state using SCF orbitals. Once again we correlated 17 electrons and used the same orbital space as in the single reference calculation, only now in addition to the SCF reference we also included all singles and doubles from a

second reference configuration formed by a single excitation from the  $\text{Cu}3d\sigma$  to  $\text{O}2p\sigma$ . This second configuration is the only additional configuration to have a coefficient greater than 0.05 in the single reference CI; it has ionicity  $\text{Cu}^{+2}$  and  $\text{O}^{-2}$ . The reference configurations were:

$$(\text{O}2s)^2 (\text{O}2p\sigma)^1 (\text{O}2p\pi)^4 (\text{Cu}3d\sigma)^2 (\text{Cu}3d\pi)^4 (\text{Cu}3d\delta)^4 - \text{SCF}$$

$$(\text{O}2s)^2 (\text{O}2p\sigma)^2 (\text{O}2p\pi)^4 (\text{Cu}3d\sigma)^1 (\text{Cu}3d\pi)^4 (\text{Cu}3d\delta)^4 - 3d\sigma \text{ to } 2p\sigma$$

For other transition metal oxides  $\text{CrO}$ ,  $\text{MoO}$ ,  $\text{NiO}$  and  $\text{PdO}$ , we have seen that the inclusion of this type of configuration (nd to 2p excitations) leads to a considerable bond shortening. However for  $\text{CuO}$  it had a very small effect. The  $^2\Sigma^+$  bond length shortened by only  $\sim 0.02$  a.u. upon going from single to multi-reference SDCl.

We have also computed the dissociation energy,  $D_e$ . It is known that for an ionic molecule<sup>15</sup> it is better to compute the  $D_e$  relative to the ions, ( $\text{Cu}^+$  and  $\text{O}^-$ ) and to correct this value with the experimental atomic ionization potential and electron affinity.<sup>16</sup> We have computed the  $D_e$  at both the SCF and CI levels and find a  $D_e$  (SCF) of 1.40 eV and a  $D_e$  (CI) of 1.88 eV. For a purely ionic system, the  $D_e$  (SCF) and  $D_e$  (CI) are extremely similar, but in  $\text{CuO}$  they differ by 0.5 eV. This is consistent with the Mulliken populations which show some covalent character. However, the CI value is much smaller than the experimentally cited value<sup>1</sup> of 2.79 eV. Even considering the errors which may arise due to the choice of basis set and level of the correlation treatment, it appears 2.79 eV is quite likely to be too large. We estimate that a better value for  $D_e$  is in the range 2.0-2.3 eV.

#### IV. ORIGIN OF THE $^2\Pi$ - $^2\Sigma^+$ SEPARATION

One important feature of  $\text{CuO}$  is the size of the lowest  $X^2\Pi$ - $A^2\Sigma^+$  separation ( $\sim 7,200 \text{ cm}^{-1}$ ). The  $\text{Cu}^+$  ion  $^1S(3d^{10})$  is a closed shell state as is  $\text{K}^+ ^1S(3p^6)$ ; but in  $\text{KO}$

the  ${}^2\Pi$ - ${}^2\Sigma^+$  separation<sup>1,2</sup> is only  $\sim 350 \text{ cm}^{-1}$ . In order to analyse the origin of this different behavior, we calculated some molecular properties for KO and CuO using SCF orbitals for  $\text{K}^+$ ,  $\text{Cu}^+$  and  $\text{O}^-$ . (For  $\text{O}^-$ , the atomic wavefunctions were computed in  $C_{\infty v}$  symmetry. We used the orbitals from the  $2p\sigma^2 2p\pi^3$  state.) The molecular properties were computed for a bond length near equilibrium;  $r=4.25$  bohr for KO and  $r=3.27$  bohr for CuO. The energies for both  ${}^2\Pi$  and  ${}^2\Sigma^+$  states were evaluated for the atomic orbitals with the  $\text{O}^-$  orbitals Schmidt orthogonalized to those of the metal ion ( $\text{K}^+$  or  $\text{Cu}^+$ ). We refer to the difference between this frozen orbital energy and the SCF energy as the relaxation energy. For KO, this relaxation energy is very small,  $\sim 5,000 \text{ cm}^{-1}$ . This is consistent with a highly ionic behavior which is characterized by a Mulliken gross charge of  $\sim 0.9e$  on K and a very small K-O overlap population of  $\sim 0.07$ . For CuO, the relaxation energies are somewhat larger,  $\sim 13,000 \text{ cm}^{-1}$ . This is consistent with a less ionic gross charge of  $\sim 0.7$  and a larger overlap population of  $\sim 0.3$ . The differential relaxation energies between the  ${}^2\Pi$  and  ${}^2\Sigma^+$  (given in Table II) are very similar for KO and for CuO; for both molecules it is rather small  $\sim 1,800 \text{ cm}^{-1}$ . These calculations support the view that  ${}^2\Sigma^+$  and  ${}^2\Pi$  states for both systems are dominantly ionic.

The origin of the separation of the  ${}^2\Sigma^+$  and  ${}^2\Pi$  states can thus be analysed in terms of integrals between the orbitals of the separated ions. We have evaluated the overlap of the  $\text{O}2p\sigma$  and  $\text{O}2p\pi$  with the metal,  $\text{Cu}^+$  or  $\text{K}^+$ , orbitals and the one electron, kinetic energy plus nuclear attraction, integrals for the oxygen p orbitals denoted  $h(2p\sigma, 2p\sigma)$  and  $h(2p\pi, 2p\pi)$ . The overlap integrals are a measure of the Pauli repulsion and the one electron integrals a measure of the nuclear attraction. To account for the shielding by the core electrons, the core potential was evaluated for the configurations  $\text{Cu}1s^2 \dots 3d^{10}$ ,  $\text{K}1s^2 \dots 3p^6$ , and  $\text{O}1s^2 2s^2$  and added to the one electron integrals. This potential is  $\sum N_i (J_i - \frac{1}{2}K_i)$ ;



$i=1s,2s,\dots$ , where  $N_i$  is the orbital occupation number and  $J_i$  and  $K_i$  are the Coulomb and exchange operators respectively. In effect, the metal atom is treated as a +1 ion. These quantities are summarized in Table II. For KO, the difference between  $h(2p\pi,2p\pi)$  and  $h(2p\sigma,2p\sigma)$  is small, however the  $\sigma$ - $\sigma$  overlap is 6 times the  $\pi$ - $\pi$  overlap. Thus for KO, the repulsion dominates and the  $^2\Sigma^+$  state which has one less  $\sigma$  electron is the lower state. Also the  $^2\Pi$  state has a longer  $r_e$ ,<sup>2</sup> this lengthening reduces the overlap repulsion. The net behavior is that the separation of these states is very small. In the CuO case, the difference in the one electron integral is 4.4 times larger than in KO. The larger value for  $h(2p\sigma,2p\sigma)$  favors the  $^2\Pi$  state which has two  $2p\sigma$  electrons. The ratio of  $\sigma$ - $\sigma$  to  $\pi$ - $\pi$  overlap is 2.5, down from 6 in KO. The lower  $\sigma$  repulsion and the increase in the  $\sigma$  nuclear attraction,  $h(2p\sigma,2p\sigma)$ , relative to  $\pi$  leads to a  $^2\Pi$  ground state and a much larger  $^2\Pi$ - $^2\Sigma^+$  separation. Also since  $\sigma$  repulsion is not as dominant a feature for CuO, the  $r_e$  for  $^2\Pi$  and  $^2\Sigma^+$  are the same at the SCF level, while for KO,<sup>2</sup> they differ by  $0.12\text{\AA}$ . Similar effects have been used to explain the  $^2\Sigma^+$ - $^2\Pi$  separation for the alkali metal monoxides.<sup>4</sup>

## V. STATES ARISING FROM $3d^9 4s^1$ MANIFOLD

To investigate the nature of the excited state spectrum of CuO, and, in particular, to identify possible candidates for the experimentally observed  $^2\Sigma^+$  state at  $\sim 16,000\text{ cm}^{-1}$ , we have performed SCF, MCSCF and SDCI calculations on several of the states in the  $3d^9 4s^1$  manifold. Our interest is to obtain qualitative information on the nature and positioning of the states in this upper manifold.

We expect the two ionic groups of this manifold,  $O^- 2p\sigma^1 2p\pi^4$  and  $2p\sigma^2 2p\pi^3$ , to be similar to the  $3d^{10}$  manifold, with the ionic  $O^- 2p\pi$  hole states lower by  $\sim 8,000\text{ cm}^{-1}$ . Each group will, of course, be split into several states because of the three possible d holes ( $\sigma$ ,  $\pi$  and  $\delta$ ) and the two different spin couplings (doublet and quartet). We have investigated

various orientations of the d holes, and for both of the ionic groups of states, as well as for the mixed group of states, we find the splitting to be small. Furthermore, we would expect the splitting between these two ionic groups to be well computed at the SCF level as was the case for the  $3d^{10}$  manifold. The third group, the mixed states, is different and it is not easy to predict their location relative to the two ionic groups. It can be considered as having one  $O2p\sigma$  electron, therefore, as an upper bound it would lie near the ionic  $O2p\sigma$  hole state; however, it is lowered by the strength of the  $Cu(4s)-O(2p\sigma)$  covalent bond. The strength of this bond is not well computed at the SCF level. The minimum treatment required is a simple MCSCF accounting for the correlation of this  $\sigma$  bond which is not present in the two ionic groups. Thus, a qualitatively accurate splitting among the groups of the  $3d^9 4s^1$  manifold should be given by SCF calculations for the two ionic groups and a simple MCSCF for the mixed group.

In addition to the splitting within this manifold, we would like to position the  $3d^9 4s^1$  manifold with respect to the  $3d^{10}$  manifold. It is known that at the SCF level, the  $Cu^2 D(3d^9 4s^2) - ^2S(3d^{10} 4s^1)$  and the  $Cu^+ ^1S(3d^{10}) - ^3D(3d^9 4s^1)$  splittings are in poor agreement with experiment (as shown in Table III) and we expect similar errors to arise in the CuO molecule. Since it is possible to clearly identify the molecular states as arising from  $3d^9$  or  $3d^{10}$ , we simply shift the computed results by a correction factor to account for the intrinsic errors in the SCF description of Cu and  $Cu^+$ . The correction ( $11,460\text{ cm}^{-1}$ ) is computed to be the weighted average of the SCF error in Cu ( $\sim 9,000\text{ cm}^{-1}$ ) and  $Cu^+$  ( $\sim 12,000\text{ cm}^{-1}$ ) based on a charge of 0.75 which is approximately that computed for CuO at the SCF level. Since the errors of Cu and  $Cu^+$  are reasonably similar, this correction would not change greatly if a somewhat different choice of ionicity were used.

At the CI level, the error in the Cu and Cu<sup>+</sup> splittings has been considerably reduced, see Table III; thus for CuO, we expect that the uncorrected CI results for the vertical separations will be quite similar to the corrected SCF (or MCSCF) results. The CI calculations serve both to refine our separations and as a check on the simple model on which the SCF/MCSCF results are based.

For the states of the 3d<sup>9</sup>4s<sup>1</sup> manifold, we carried out all calculations at R(Cu-O)=1.73Å, the experimental  $r_e$  of the X<sup>2</sup>Π state.<sup>1</sup> The  $r_e$  for all observed states is very similar<sup>1</sup> and hence we felt that the excited states could be computed at one point.

The three different states of the mixed group were evaluated at the SCF level and the results are summarized in Table IV. We find the splitting among them is only 0.4 eV. We also found similar splittings, upon changing the orientation of the d hole, in the two ionic groups, thus for further calculations we considered only a single <sup>2</sup>Π state for each group as representative of all of the states in the group. The <sup>2</sup>Π symmetry for the representative state was chosen for computational convenience.

The MCSCF wavefunctions were obtained using the CASSCF technique.<sup>6</sup> In this approach the orbitals are divided into inactive orbitals, which are doubly occupied in all configurations and active orbitals which are occupied with all possible symmetry allowed distributions of the active electrons. The same MCSCF was performed for all three <sup>2</sup>Π states. It consists of 5 active electrons with 2 active σ and 1 active π orbital. We have also imposed the restriction of 2 electrons in the σ space and 3 in the π. This leads to 4 configurations. (Symmetry and equivalence restrictions were imposed for the π but not for the δ orbitals. We tested the importance of this constraint with the SCF wavefunctions and found it to lead to changes in the energy of less than 0.2 millihartrees.) For the mixed state,

the active  $\sigma$  orbitals are the bonding and anti-bonding combinations of Cu, dominantly 4s and O2p $\sigma$  orbitals; the active  $\pi$  orbital is essentially Cu3d $\pi$ . For the ionic O2p $\sigma$  hole state the active  $\sigma$  orbitals are essentially Cu4s and O2p and the active  $\pi$  is 3d $\pi$ . For the ionic O2p $\pi$  hole state the active orbitals are Cu4s $\sigma$ , Cu3d $\sigma$  and O2p $\pi$ . This choice of active orbitals and electrons leads to a large correlation effect,  $\sim 14,000 \text{ cm}^{-1}$ , for the mixed state (see Table V) which is typical of a covalent bond. For the two ionic states we have effectively performed an SCF calculation since a single CSF (configuration state function) has a weight of  $>0.99$ . The corrected vertical excitation energies from these calculations,  $\Delta'$  in Table V are  $\sim 15,000 \text{ cm}^{-1}$  for the mixed and ionic O2p $\pi$  hole states, the O2p $\sigma$  hole state is much higher at  $\sim 27,000 \text{ cm}^{-1}$ .

The SDCI calculations for these states were performed with the same number of deleted virtual and frozen, doubly occupied, core orbitals as for the calculations on the 3d<sup>10</sup> manifold. The orbitals used were those from the MCSCF calculations described above. The excitations were made from only one component of the degenerate <sup>2</sup> $\Pi$  state. For the two ionic states, the single and double excitations were made from a single configuration, these CSF's are shown in Table V. The mixed state excitations were made from two CSF's, one is shown in Table V and the second is formed by replacing the bonding (4s+O2p $\sigma$ )<sup>2</sup> with the anti-bonding (4s-O2p $\sigma$ )<sup>2</sup> in this CSF. The CI vertical excitation energies,  $\Delta$  in Table V, are given as calculated without correction.

The difference between the MCSCF and CI results for the separation of the ionic states and for the CI  $\Delta$  and the corrected MCSCF  $\Delta'$  are rather small. This is consistent with the small difference between the SCF and CI separations for the 3d<sup>10</sup> X<sup>2</sup> $\Pi$  and A<sup>2</sup> $\Sigma^+$  states. It also follows because the CI leads to a very small mixing between 3d<sup>10</sup> and 3d<sup>9</sup>4s<sup>1</sup> configurations. There is some change between the MCSCF and CI results for the mixed

state, the CI  $\Delta$  is  $\sim 3,000 \text{ cm}^{-1}$  less than the MCSCF  $\Delta'$ . Although the MCSCF wavefunction is able to qualitatively describe the bonding pair, the extensive correlation of the SDCI treatment is needed to position this state more accurately. This CI treatment brings the mixed and the ionic  $\text{O}2\text{p}\pi$  hole states virtually on top of each other. We conclude that the state, observed<sup>1</sup> at  $\sim 15,000 \text{ cm}^{-1}$  is either a mixed state or an ionic  $\text{O}2\text{p}\pi$  hole state. The ionic  $\text{O}2\text{p}\sigma$  hole state is too high to be considered. The separation between the  $\text{O}2\text{p}\pi$  hole and  $\text{O}2\text{p}\sigma$  hole ionic states is larger than in the  $3\text{d}^{10}$  manifold. We assume that this is because the  $\text{O}2\text{p}\pi$  hole state has only one  $3\text{d}\sigma$  electron thus reducing the  $\sigma$  overlap and further enhancing the nuclear attraction preference for the  $\text{O}2\text{p}\pi$  hole over the  $\text{O}2\text{p}\sigma$  hole state.

We should note that our MCSCF and CI calculations for this manifold do not satisfy McDonald's theorem. Both the mixed and ionic  $\text{O}2\text{p}\pi$  hole states were the lowest roots of the CASSCF calculation, while the ionic  $\text{O}2\text{p}\sigma$  hole state was optimized as a second root. In all cases, the lowest root of the CI was selected. The fact that the lowest roots are  $3\text{d}^9 4\text{s}^1$  like and not  $3\text{d}^{10}$  like follows simply because the orbitals for the appropriate states of the Cu atom and the  $\text{Cu}^+$  ion are different. If the one configuration energy of  $\text{Cu } ^2\text{D}(3\text{d}^9 4\text{s}^2)$  is evaluated using the SCF orbitals determined for  $\text{Cu } ^2\text{S}(3\text{d}^{10} 4\text{s}^1)$ , the separation between them is 4.70 eV. If separate SCF calculations are performed for the  $^2\text{S}$  and  $^2\text{D}$  states, the separation is 0.37 eV. A CI calculation based on a common set of orbitals for these states would have to be very large to describe these large orbital relaxation effects. Our CI calculations ( $\sim 100,000$  configuration) were not yet large enough to account for them. Thus each SDCI calculation was based on individually optimized orbitals from the appropriate MCSCF wavefunctions. This accounts for the relaxation simply and in a compact fashion. Since the CI's for the  $3\text{d}^{10}$  manifold do not appear to mix in much  $3\text{d}^9 4\text{s}^1$  character, we feel

the fact that there is no lower  $3d^{10}$  like root in these calculations is not a severe problem. That the ionic  $O2p\pi$  hole and the mixed states are virtually identical in energy and that each is the lowest root is a potential problem. However, we feel that we have shown that the state observed at  $\sim 15,000\text{ cm}^{-1}$  is due to either a mixed or an ionic  $O2p\pi$  hole state and that the ionic  $O2p\sigma$  hole state is much higher up. It is certainly true that a more extended calculation might lead to a mixing, and hence somewhat separate the mixed and  $O2p\pi$  hole states. However, this is outside our goal of qualitative understanding of the  $3d^9 4s^1$  manifold.

## VI. CONCLUSIONS

There is an unobserved  $^2\Sigma^+$  state at  $\sim 8000\text{ cm}^{-1}$  arising out the the  $Cu^+ 3d^{10}$  manifold. The previously identified  $A^2\Sigma^+$  is probably a state arising from the  $Cu^+ 3d^9 4s^1$  manifold. While we have performed calculations on  $^2\Pi$  states, we expect these to lie close to the  $^2\Sigma^+$  states, since our tests on the  $3d^9 4s^1$  manifold indicate that the energy of the state is reasonably independent of the position of the d hole. We found both the mixed state and the ionic state with an  $O2p\pi$  hole to be positioned at  $\sim 15,000\text{ cm}^{-1}$ , and considered these as two candidates for the experimentally observed state. The third type of state in the  $3d^9 4s^1$  manifold,  $Osp\sigma$  hole, is at  $\sim 30,000\text{ cm}^{-1}$ .

A comparison with KO shows that while the d's are not directly involved in the chemical bonding, their presence leads to a change in the ratio of the  $\sigma$  one electron integrals to those of  $\pi$  symmetry. The  $\sigma$  are closer to the  $\pi$  overlap integrals for CuO than for KO. The  $\sigma$  one electron integral is also considerably smaller than the  $\pi$  integral. Thus, for CuO, both the nuclear attraction significantly favors the  $^2\Pi$  state and the Pauli repulsion bias against it is reduced.

TABLE I

The SCF and CI results for the  $X^2\Pi$  and  $A^2\Sigma^+$  states of the  $3d^{10}$  manifold. The properties given are the equilibrium Cu-O bond distance,  $r_e$ , the vibrational frequency,  $\omega_e$ , and the dissociation energy,  $D_e$ . Also given are the total energy,  $E$ , the energetic separation of the states,  $\Delta$ , and the correlation energy obtained for the SDCi wavefunctions. The energies are those computed at the appropriate  $r_e$ 's.

		$^2\Pi$	$^2\Sigma^+$	$\Delta$ (cm $^{-1}$ )
SCF	$r_e$ (Å)	1.875	1.875	
	$E$ (a.u.)	-1713.59823	-1713.56546	7190
	$\omega_e$ (cm $^{-1}$ )	527.	488.	
	$D_e$ (eV)	1.40	--	
CI	$r_e$	1.82	1.81	
	$E$	-1713.99679	-1713.95889	8320
	$\omega_e$	545.	534.	
	$D_e$ (eV)	1.88	--	
	$E_{\text{corr}}$ (eV)	10.85	10.71	
Experiment <sup>a</sup>	$r_e$	1.724	--	
	$\omega_e$	640.17	--	
	$D_e$ (eV)	2.79	--	

<sup>a</sup>See Ref. 1.

TABLE II

Tabulation of the one electron properties for KO and CuO. For the Mulliken populations the gross charge is followed by the overlap charge in parentheses. The energies of the  $^2\Pi$  and  $^2\Sigma^+$  molecular states are also given; the SCF energy is compared to the frozen orbital energy obtained with the orbitals of the separated ions. The  $^2\Pi$  and  $^2\Sigma^+$  separation,  $\Delta$ , is computed in both ways.

	CuO r=3.27 a.u.		KO r=4.25 a.u.	
Muliken Populations				
$^2\Pi$ O population	0.719	(0.295)	-0.909	(0.071)
$^2\Sigma^+$ O population	0.771	(0.263)	-0.923	(0.004)
Overlap Integrals				
$\langle O2p\sigma   Cu3d\sigma \rangle$	0.091			
$\langle O2p\sigma   Cu3p\sigma \rangle$	0.081	$\langle O2p\sigma   K3p\sigma \rangle$	0.149	
$\langle O2p\sigma   Cu3s \rangle$	0.126	$\langle O2p\sigma   K3s \rangle$	0.142	
$\langle O2p\pi   Cu3d\pi \rangle$	0.088			
$\langle O2p\pi   Cu3p\pi \rangle$	0.030	$\langle O2p\pi   K3p\pi \rangle$	0.050	
One Electron Integrals (Hartrees)				
$h(2p\sigma,2p\sigma)$	-3.0726		-2.9108	
$h(2p\pi,2p\pi)$	-2.9554		-2.8842	
Energies				
SCF $^2\Pi$ (Hartrees)	-1713.59147		-673.94486	
Frozen orb. $^2\Pi$	-1713.53085		-673.92844	
Relaxation ( $cm^{-1}$ )	13303.		3603.	
SCF $^2\Sigma^+$ (Hartrees)	-1713.55972		-673.94679	
Frozen orb. $^2\Sigma^+$	-1713.50738		-673.92211	
Relaxation ( $cm^{-1}$ )	11486.		5416.	
$\Delta$ SCF ( $cm^{-1}$ )	7089.		425.	
$\Delta$ Frozen ( $cm^{-1}$ )	5151.		1390.	



TABLE III

Summary of Cu and Cu<sup>+</sup> calculations.  
 The separation,  $\Delta$ , is in wavenumbers and the total energy in Hartrees.

	E(3d <sup>9</sup> 4s <sup>2</sup> )	Cu E(3d <sup>10</sup> 4s <sup>1</sup> )	$\Delta$	E(3d <sup>10</sup> 4s <sup>1</sup> )	Cu <sup>+</sup> E(3d <sup>10</sup> )	$\Delta$
NHF <sup>a</sup>	-1638.9505	-1638.9662	3450	-1638.6814	-1638.7287	10380
SCF	-1638.7611	-1638.7749	3033	-1638.4915	-1638.5393	10490
SDCI	-1638.9775	-1638.0248	10374	-1638.6741	-1638.7729	21690
EXP <sup>b</sup>			12020			22649

<sup>a</sup>Numerical Hartree Fock.

<sup>b</sup>Ref. 7.

TABLE IV

SCF energies (in Hartrees) for the three mixed states arising from the  $3d^9 4s^1$  manifold, calculated at  $r=3.27$  a.u.

State	Valence Configuration	Energy
$^2\Sigma^+$	$(4s+O2p\sigma)^2 3d\sigma^1 3d\pi^4 3d\delta^4 O2p\pi^4$	-1717.50912
$^2\Pi$	$(4s+O2p\sigma)^2 3d\sigma^2 3d\pi^3 3d\delta^4 O2p\pi^4$	-1713.50494
$^2\Delta$	$(4s+O2p\sigma)^2 3d\sigma^2 3d\pi^4 3d\delta^3 O2p\pi^4$	-1713.49360

TABLE V

SCF, MCSCF and SDCI energies (in Hartrees) and vertical excitation energies,  $\Delta$ , (in  $\text{cm}^{-1}$ ) for the three types of  $^2\Pi$  states arising from the  $3d^9 4s^1$  manifold and the  $^2\Pi$  state arising from the  $3d^{10}$  manifold. All states are calculated at  $r=3.27$  a.u. For the CI, the weight of the SCF configuration is given in parentheses. SCF and MCSCF vertical excitation energies corrected for the  $3d^{10}$ - $3d^9 4s^1$  separation error,  $\Delta'$ , are also reported.

	Energy	$\Delta$	$\Delta'$
A. $3d^{10}$ State, $X^2\Pi$ - $3d\sigma^2 3d\pi^4 3d\delta^4 O2p\sigma^2 O2p\pi^3$			
SCF	-1713.59823		
CI	-1713.99679 (0.91)	0	0
B. $3d^9 4s^1$ Mixed State- $(4s+O2p\sigma)^2 3d\sigma^2 3d\pi^3 3d\delta^4 O2p\pi^4$			
SCF	-1713.50493	20,480	31,940
MCSCF	-1713.57022 (0.82)	6,150	17,610
CI	-1713.9325 (0.85)	14,110	
C. $3d^9 4s^1 O2p\sigma$ Hole- $4s^1 3d\sigma^2 3d\pi^3 3d\delta^4 O2p\sigma^1 O2p\pi^4$			
MCSCF	-1713.52615 (0.99)	15,820	27,280
CI	-1713.8730 (0.91)	27,170	
D. $3d^9 4s^1 O2p\pi$ Hole- $4s^1 3d\sigma^1 3d\pi^4 3d\delta^4 O2p\sigma^2 O2p\pi^3$			
MCSCF	-1713.58735 (0.99)	2,390	13,850
CI	-1713.9322 (0.91)	14,180	

## REFERENCES

1. K. P. Huber and G. Herzberg, Constants of Diatomic Molecules, (Van Nostrand, New York, 1979).
2. S. P. So and W. G. Richards, *Chem. Phys. Letters* **32**, 227 (1975).
3. C. E. Moore, *Atomic Energy Levels*, Natl. Bur. Stand. (US), cir. 467 (1949). All energies are given as the weighted average over J values.
4. (a) B. C. Laskowski, S. R. Langhoff and P. E. M. Siegbahn, *Int. J. Quantum Chem.*, (in press). (b) J. N. Allison and W. A. Goddard III, *J. Chem. Phys.* **77**, 4259 (1982).
5. The MOLECULE integral program was written by J. Almlöf at the University of Uppsala, Sweden. The ALCHEMY SCF and integral ordering and transformation programs were written by P. S. Bagus, B. Liu and M. Yoshimine at the IBM Research Laboratory, San Jose.
6. B. O. Roos, P. R. Taylor and P. E. M. Siegbahn, *Chem. Phys.* **48**, 157 (1980).
7. P. E. M. Siegbahn, *J. Chem. Phys.* **72**, 1647 (1980); **70**, 6391 (1979).
8. A. J. H. Wachters, *J. Chem. Phys.*, **52**, 1033 (1970).
9. P. J. Hay, *J. Chem. Phys.* **66**, 4377 (1970).
10. T. H. Dunning Jr., *J. Chem. Phys.* **53**, 2823 (1970).
11. T. H. Dunning Jr. and P. J. Hay, *Methods of Electronic Structure Theory*, H. F. Schaefer III, ed., pp. 1-27, (Plenum Press, New York, 1977). The recommended d exponent for O is  $\alpha = 0.85$  rather than 0.90 which we have used.
12. NiH - See for example: (a) P. S. Bagus and C. Bjorkman, *Phys. Rev. A* **23**, 461 (1981). (b) S. P. Walch and C. W. Bauschlicher Jr., *Chem. Phys. Letters* **86**, 66 (1982). (c) M. R. A. Blomberg, P. E. M. Siegbahn and B. O. Roos, *Mol. Phys.* **11**(1) (1982).
13. Cu<sub>2</sub> - See for example: C. W. Bauschlicher Jr., S. P. Walch and P. E. M. Siegbahn, *J. Chem. Phys.* **76**, 6015 (1982).

14. Other transition metal hydrides - see for example: S. P. Walch and C. W. Bauschlicher Jr., submitted for publication.
15. (a) C. W. Bauschlicher Jr., B. H. Lengsfeld and B. Liu, *J. Chem. Phys.* **77**, 4084 (1982). (b) B. H. Lengsfeld and B. Liu, unpublished results. (c) C. W. Bauschlicher Jr. and H. Partridge, *Chem. Phys. Letters*, (in press).
16. H. Hotop and W. C. Lineberger, *J. Phys. and Chem. Ref. Data.* **4**, 530 (1975).

The following is the final technical report of Dr. A. Komornicki and was written by Dr. Jan Almlof of the Department of Chemistry University of Oslo, Norway. This work was carried out from December 1983 through February 1985. This report is the third and final part of the final report on NASA Grant NCC2-158.

N86-29929<sup>D5-25</sup>

269.

18319

A VECTORIZED MOLECULE CODE

Ø 2736708

Final report on a project supported by  
the NASA Ames grant no. NCC2-158.

by Jan Almlöf

Department of Chemistry  
University of Oslo  
0315 Oslo 3, Norway.

## Contents

1	Background and aim of the work	1
2	General considerations	2
3	Comparison with the old code	4
4	Memory management	5
5	Computational simplifications	7
6	Contraction	10
7	Specific difficulties encountered	12
8	Guide for users	14
9	Plans for future development	17
	References	19
	Appendix A: Definitions and abbreviations	20
	Appendix B: Input description	21



## 1. Background and aim of the work

The original MOLECULE integral program was written in 1971-1972 /1/. With minor modifications /2/, it has been used by quite a number of scientists around the world, and it has been implemented on many different computer systems. On the scalar machines available in the 70's - and for the basis sets generally considered adequate at that time - it performed rather well. The fact that it produces integrals over a symmetry-adapted basis still makes it an attractive alternative for many types of applications.

The ongoing development of vector-oriented computers and the increasing use of large basis sets with high  $l$ -values places new demands on an efficient integral program. In order to run efficiently the code should be organized such that it benefits from the specific features of modern hardware, e.g. parallelism, pipelining and special vector-oriented instruction sets. This is not the case with the old version of MOLECULE, and accordingly it doesn't run efficiently on supercomputers such as the CRAY-1 or CYBER-205.

The aim of the present work has been to produce an integral code suited for modern, vector-oriented hardware, in particular for the CRAY series of computers. It should be capable of handling basis functions with high angular quantum numbers in an efficient way. The code is assumed to replace the old MOLECULE program, and a reasonably compatible in- and output has therefore been a desire.

## 2. General considerations

The term "vectorization" is normally used for the process of adapting computer code to vector-oriented hardware. This usually amounts to modifying the code to make it benefit from the special vector-handling facilities available on modern computers. In a vectorized program, a major portion of the computational work should be performed in simple loops of sufficient length to utilize these facilities in an optimum way.

In many cases, the vector structure is inherent in the algorithms and the original code. Vectorization then amounts to cleaning up the innermost loops, removing IF-tests and subroutine calls, minimizing I/O, etc.

In other cases, however, the vector structure is not evident from the algorithm. The kernel of the code may be scalar, highly branched or contain loops of insufficient length. The execution is repeated through long outer loops over large portions of code, which do not invoke the use of special vector instructions.

The two situations briefly described above are often referred to as "intrinsic" and "extrinsic" vectorization cases. Clearly the extrinsic vectorization is by far the more difficult one, as it requires changing the structure of the entire code - sometimes also of the algorithms.

Many tasks involving manipulation of vectors and matrices can be performed in alternative ways. If the algorithm contains nested

loops there is usually a freedom of choice as to the order of these loops. The optimum choice may be dependent on input parameters, e.g. on vector lengths, but also on the type of hardware used. The task of multiplying two rectangular matrices may serve as an example. In the triple-nested loop constituting the kernel of such an operation, one would normally choose the longest loop as the innermost one in order to obtain efficient vector performance. In some cases, however, that would amount to evaluating each element in the result matrix as a dot product. That scheme, while allowing peak performance on an FPS164, would not vectorize at all on true vector machines like the CRAY or CYBER-205. Of the two other possibilities, only one would perform well on a CYBER-205 due to problems with a vector stride larger than one. The comparison is further complicated by the fact that the latter two schemes may exploit the sparseness of the initial matrices, which the scalar product does not.

Evidently, it is not always possible to design a straightforward algorithm which is both optimized and portable. Our approach to the problem has been to code routines for such standard elements of computation, which involve several alternative possibilities. The final choice, made at execution time, is dependent on the loop lengths, and, in addition, on parameters in the code which may be optimized at each installation, depending on the hardware used and the type of problem for which optimum performance is desired.

### 3. Comparison with the old code

The original MOLECULE code is a typical case for extrinsic vectorization. The innermost, easily recognizable loop structure is the nest of four loops over primitive GTOs which together make up one integral over contracted functions. Inside these loops there are some 1000-1500 lines of code. Extensive testing and branching is performed to take advantage of the simplifications due to low quantum numbers, planar molecular fragments, etc. Calls to external routines also hinder the vectorization.

The integrals over GTOs are evaluated in batches, made up by all integrals within a quadruple of GTSs (see Appendix A for definitions). This saves recomputation of several quantities, but the loops generating these batches are not well suited for vectorization. To get loops of sufficient length it was found necessary to change the entire structure of the program.

In the new code, all GTOs on a center with a given  $l$ -value are considered as a group (GGTO). Certain compromises and modifications of that approach may be necessary due to finite memory size, as discussed further below. The innermost loops in the integral code is made over groups involving all integrals over functions in four such GGTOs. The vector length for those operations will become  $N_4 = n_1 \cdot n_2 \cdot n_3 \cdot n_4$ ;  $n_i$  being the number of GTOs in the  $i$ :th group. In a very schematic way, one may view the new procedure as derived from the old one by replacing every scalar operation in the kernel by a vector loop of length  $N_4$ .

#### 4. Memory management

The dimensioning of arrays in an integral code requires some special attention. Different arrays may become very large in different situations, depending on the quantum numbers, degree of symmetry, number of primitive functions in one contracted, etc. Dimensioning each array to the largest size attained in routine applications would quickly blow up the memory of most computers.

On the other hand, it is quite unlikely that these arrays would all be large at the same instant of execution. (A molecule with eight symmetry-related atoms, each with five or six f-functions contracted to one is not a likely candidate for routine calculations). Our approach has therefore been to use a truly dynamic allocation of memory. All large arrays are stored in two main working areas, and have variable dimensions which are passed in the subroutine calls. The array boundaries are allowed to change at execution time. With this arrangement each array takes only the space needed at any particular instant. In addition, temporary arrays used at different stages of the calculation are allowed to overlap.

However, even with maximum packing of arrays at any given instant, memory limitations may be encountered. This is rather easily handled for the case of segmented contraction. In that case, the loops over primitive integrals may be divided into several passes, using a "strip-mining" technique. In each pass, one computes only the portion of primitive integrals which can be easily handled in the available memory. It is trivial to sum

these integrals as they arrive, in order to make up a contracted integral, and this step is hardly affected at all by the strip-mining.

For the general contraction case, however, one would need all the primitive integrals before starting the transformation, but clearly this is not always feasible. The situation is further complicated as the program takes certain shortcuts whenever two or more of the GGTOs involved are the same. Apparently, the permutational symmetry present in the full integral set for such cases will be obscured if only part of the set is considered at a time.

We have introduced a rather reasonable compromise in order to tackle this problem. In the segmented contraction case the effective vector length is  $n_1 \cdot n_2 \cdot M$ ;  $M$  ranging between 1 and  $n_3 \cdot n_4$  depending on the memory available. For general contraction, however, the choice of  $M$  had to be restricted to the values 1,  $n_3$  or  $n_3 \cdot n_4$ . (The  $n_i$ 's are defined in Section 3).

## 5. Computational simplifications

In any computational work, it is customary before time-consuming sub-tasks are performed, to test whether the results of the sub-task will significantly affect the final result.

When evaluating molecular integrals there is an almost unlimited number of special cases which may be treated with fewer numerical operations than the general case, and which, accordingly, are candidates for such tests. Simplifications may arise due to  $n$ -center cases with  $n < 4$ , for integrals involving linear or planar fragments, for low angular quantum numbers, or because small multiplicative prefactors make the evaluation unnecessary. Simplifications also arise due to global - or local - symmetry (of which linear and planar fragments are examples).

The extent to which pre-testing is worthwhile depends on the efficiency with which the test can be performed, the hit-rate of such a test, the complexity of the operations to be avoided and on possible degradation of program efficiency as a result of such testing.

In the old program, integrals are computed in batches associated with a quadruplet of shells. Within a batch, the product of radial overlaps

$$T_{\mu\nu\lambda\sigma} = S_{\mu\nu} S_{\lambda\sigma} \quad (1)$$

is a common factor which largely determines the magnitude of all

integrals in the batch. By comparing this factor against a threshold,

$$T_{\mu\nu\lambda\sigma} < \epsilon \quad (2)$$

a single test may eliminate the evaluation of an entire block. With that scheme used in the new code, the testing would have occurred in the innermost loops over GTOs, and it would have inhibited vectorization completely. A different approach has therefore been taken:

Initially, the sub-ranges of elements  $T_{\mu\nu\gamma\sigma} > \epsilon$  are determined for all  $T_{\mu\nu\gamma\sigma}$  within the group to be processed.  $T$ , and all other 4-index quantities necessary for the integral evaluation are then compressed into smaller arrays, based on those sub-ranges. The operation is nearly identical to the Q8VCMPRS on the CYBER-205, but since few other vendors offer that possibility we have coded it in Fortran. After compressing all arrays the integrals are evaluated, usually a smaller number than the full  $N_4$  set. In cases of general contraction it is necessary to return to the full, ordered set of  $N_4$  integrals before transforming to the contracted basis. This is achieved by expanding the array with the inverse operation, which again is very similar to the Q8VXPND on the CYBER-205.

The old program made extensive use of special code for low quantum numbers. This led to substantial savings for certain types of integrals, as compared to the general procedure. With a vectorized code the gain may be less, as the overhead in the general



scheme is amortized over a large number of integrals. Furthermore, in most time-critical applications today integrals with low quantum numbers play a minor role, anyway. We have therefore chosen to develop a first version without special routines, apart from some specific coding for ssss-type integrals. However, a vectorized code for low quantum numbers is in preparation, and will be implemented in the future.

The simplifications due to local - or global - symmetry are treated outside the innermost loops, and may therefore be retained in the new code without degradation of performance. The situation when two or more GGTOs are the same is handled by folding the arrays of radial overlap -  $S_{\mu\nu}$  and/or  $S_{\lambda\sigma}$  in (1) - whenever they are symmetric. The resulting zeros in  $T_{\mu\nu\lambda\sigma}$  will then be removed by the COMPRESS feature of the program, which in turn enhances the speed.

## 6. Contraction

The segmented contraction scheme (i.e. any primitive function contributing to only one contracted function) seems to present a problem on modern vector hardware, in the sense that it is difficult to obtain efficient vectorization. The general contraction scheme /3,4/ is more favourable in this respect; however, care must still be taken in order to achieve optimum performance. Apparently, a four-index  $n^5$  transformation scheme involves the minimum number of operations. On the other hand, the index range in each step of the procedure will be too short to permit efficient vectorization. The transformation has therefore been arranged so that in any quarter-transformation the loops over the indices involved in the transformation are done outside the loops over the three passive indices. This has been achieved by performing the transformation steps

$$[\alpha\beta\ \gamma\delta] \rightarrow [\mu\beta\ \gamma\delta] \rightarrow [\mu\nu\ \gamma\delta] \rightarrow [\mu\nu\ \lambda\delta] \rightarrow [\mu\nu\ \lambda\sigma] \quad (3)$$

using as index quadruples

$$(\alpha, \beta, \gamma, \delta) , (\beta, \gamma, \delta, \mu) , (\gamma, \delta, \mu, \nu) , \\ (\delta, \mu, \nu, \lambda) , (\mu, \nu, \lambda, \sigma) \quad (4)$$

respectively, where  $\alpha, \beta, \gamma, \delta$  represent primitive functions,  $\mu, \nu, \gamma, \sigma$  contracted functions, and the index  $(\alpha, \beta, \gamma, \delta)$  denotes storage with the first index running fastest, etc. With  $n_1, n_2$ , etc. primitives involved, and  $m_1, m_2$ , etc. contracted functions, a compressed passive index is defined from the first three

indices of a quadruple in (4), say for  $(\beta, \gamma, \delta, \mu)$  as

$$p = \gamma + (\delta-1) n_3 + (\mu-1) n_3 n_4 \quad (5)$$

Given the running order of the various indices mentioned above, the location for the integrals  $[\mu\beta \gamma\delta]$  and  $[\mu\nu \gamma\delta]$  involved in this particular quarter-transformation is given by

$$\beta + (p-1) \cdot n_2 \quad (6)$$

and

$$p + (v-1) \cdot n_3 \cdot n_4 \cdot m_1 \quad (7)$$

These integrals are accessed in a regular way, with the innermost loops over  $\mu$ ,  $\gamma$  and  $\delta$  collapsed into a single loop over  $p$ . This general contraction scheme vectorizes efficiently on a computer where contiguous vectors are not necessary, such as the CRAY. The vector lengths range between  $m_1 \cdot m_2 \cdot m_3$  and  $n_2 \cdot n_3 \cdot n_4$ .

## 7. Specific difficulties encountered

When the project was initiated, we anticipated to have access to the CRAY-1 in Sweden from late 1983 for program development and testing. The CRAY was delayed, however, and when it arrived we found the use of it extremely cumbersome due to bureaucratic obstacles of various kind.

The code has therefore been largely developed on conventional mini- and mainframe computers, with or without an attached FPS164. Only occasionally we have taken it for testing on the CRAY. In retrospect, however, this turned out not to be as serious a drawback as we had feared. Far more time was spent on a complication of an entirely different nature:

The original plans were to produce a code that would offer the same possibilities as the old MOLECULE program, apart from a substantial speed-up due to vectorization over a large number of primitive integrals. However, with all these primitive integrals available simultaneously, the possibility of a general contraction scheme seemed rather obvious. This option of performing a general contraction was originally viewed as an extra little benefit from the new organization, to be exploited whenever possible considering other restrictions. Only later did we realize the full power of the general contraction scheme. As it turns out, it provides quite a high-quality description of the atomic core even with a minimal basis representation. This seemed extremely attractive for large-scale post-Hartree Fock calculations on systems with heavy atoms, where it is important to keep the

number of basis functions as low as possible. We therefore decided to make the general contraction scheme an integrated, fully supported feature of the new program. This brought some rather serious problems to the organization and design of the new code. Solving these, as discussed in Sections 4-6, without degrading the general performance of the program, required a rather delicate analysis and some elaborate programming, and delayed the project a lot. We feel, however, that the resulting code was worth the effort spent on it. In its present status it is capable of handling virtually any reasonable basis set within a memory of 0.5-1.0 MW, and most cases with a lot less than that.

## 8. Guide for Users

This section is not intended to be the final program documentation, to be used as a program manual (such a documentation is being produced and will be distributed soon). Here we just report some of the experience gained so far, along with some remarks, hints and warnings which may be helpful when trying to install and use the code in its present shape.

As mentioned in Section 3, the primitive integrals are calculated in groups. Such a group may consist of integrals to be combined in a contraction scheme, either of segmented or general type. However, in most standard basis sets a large fraction of the basis functions consist of one primitive only. This would produce too short vectors to be of practical use if the above strategy were rigorously followed. Such "solitary" functions should therefore be grouped together and formally contracted by a one-to-one transformation. The program will recognize such a dummy contraction and take shortcuts to avoid unnecessary overhead. For optimum performance, the degree of such dummy contraction (in other words, whether e.g. six solitary functions should be combined to one, two or three groups) must be tuned to the hardware used.

The size of the working areas are set in the main program. For best performance in large-scale applications, these should be set as large as conveniently allowed, considering other limitations and restrictions in the computing environment. Note, that for large applications it may be necessary to upgrade some of the

small arrays. These are not dynamically allocated, and must be changed in a consistent way in all COMMON statements throughout the program.

If the memory allocated should be insufficient, despite the features described in Section 4, the program will normally stop after a short message is issued. This procedure is not 100 % fool-proof, and some care should be executed when large basis sets are being used.

As mentioned above, it is good policy to treat the primitive functions in groups, whether they are to be contracted or not. The number of final, contracted functions in such a group should not be too large. For instance, as an example, a contraction group involving e.g. three contracted functions of F-type (irrespective of the number of primitives) would require  $3^4 \cdot 10^4 = 810\,000$  words of storage in order to accomodate the contracted ffff-integrals. treat the primitive functions in groups, whether they are to be contracted or not. The number of final, contracted functions in such a group should not be too large. For instance, as an example, a contraction group involving e.g. three contracted functions of F-type (irrespective of the number of primitives) would require  $3^4 \cdot 10^4 = 810\,000$  words of storage in order to accomodate the contracted ffff-integrals.

In most cases, the alarm for insufficient memory will not be alerted until an integral block which violates memory limitations is treated. For obvious reasons, it is wise to place the heavy atoms first in the input sequence, such that a possible crash is encountered early in the calculation.



## 9. Plans for future development

The present code is supposed to be a first prototype useful for production calculations. A number of changes and additions are planned, however, which are going to increase its usefulness in different respects. Below, we list a number of the features which are under development:

- a) Special code for low quantum numbers. See Section 5 or a further discussion on this topic.
- b) New strategy for high quantum numbers with few primitives. The present code performs best for angular quantum numbers in the medium range (s, p, and d functions), and when the number of primitives is sufficient to allow for efficient vectorization. For solitary primitive functions with high L there are better strategies, which vectorize over sums of L-values rather than over primitive integrals. We are presently working on a code using the method of McMurchie and Davidson /5/, which will be added to the program in the future.
- c) Vectorization over symmetry-related integrals. In many cases it will be possible to increase the effective vector length - and thus the performance of the program - by treating some or all symmetry-related integrals in the same batch. This will require relatively few changes of the code, and steps are already being taken to prepare for such a modification.

d) Direct SCF implementation.

The Direct SCF technique /6/ offers interesting possibilities for very large SCF calculations, particularly in a combination with the CPU-power available on modern hardware. However, the present version, as implemented in the program DISCO, uses the old MOLECULE integral routines. Replacing these by the newly written code will drastically increase the size of molecules that can be studied with this technique.

## REFERENCES

1. J. Almlöf: "Methods for a rapid evaluation of electron-repulsion integrals in large-scale LCGO calculations". Proceedings of the second seminar computational problems in quantum chemistry, Strasbourg (1972), 14-25.
2. J. Almlöf: "The program system MOLECULE: Integral section", USIP Report 74-29 (Stockholm 1974).
3. C.M. Reeves and M.C. Harrison: "Use of Gaussian functions in the calculation of wavefunctions for small molecules". J. Chem. Phys. 39, 11-17 (1963).
4. R.C. Raffenetti: "General contraction of Gaussian atomic orbitals: Core, valence, polarization and diffuse basis sets; Molecular integral evaluation". J. Chem. Phys. 58, 4452-4458 (1973).
5. L.E. McMurchie and E.R. Davidson: "One- and two-electron integrals over Cartesian Gaussian functions". J. Comp. Phys. 26, 218-231 (1978).
6. J. Almlöf, K. Faegri, Jr. and K. Korsell: "Principles for a Direct SCF approach to LCAO-MO ab-initio calculations". J. Comput. Chem. 3, 385-399 (1982).

Appendix A. Definitions and abbreviations.

- 1) A GTO (Gaussian Type Orbital) is a primitive Cartesian Gaussian function:

$$\chi_A(r) = (x-x_A)^i (y-y_A)^j (z-z_A)^k \exp(-A(r-r_A)^2) \quad (1)$$

- 2) A CGTO (Contracted GTO) is a linear combination of GTOs on the same center  $r_A$  and with the same 'quantum' numbers  $i$ ,  $j$ , and  $k$  (i.e. differing in the orbital exponent  $A$  only).
- 3) A GTS is a shell of GTOs, i.e. a set of GTOs differing only in the quantum numbers  $i$ ,  $j$  and  $k$ . A complete set is made up by all combinations of  $i$ ,  $j$  and  $k$  subject to the restriction  $i+j+k = L$ . This leads to a set of  $\binom{L+2}{2}$  functions, or 1, 3, 6, 10, and 15 functions for  $L = 0, 1, 2, 3$ , or 4.
- 4) A CGTS is a similar shell of CGTOs.
- 5) A GGTO is a group of GTOs used in a contraction as described in 2) above.
- 6) A GGTS, similarly, is a group of GTSs (i.e. a shell of GGTOs).

Appendix B. Input description for MOLECULE (1984 version).

All input is given in free format.

Record 1: Arbitrary title.

Record 2: NTYP, NSOP, (SYM(I), I=1, NSOP), XLIM, IUNIT, IPR

NTYP = number of different types of atoms (i.e.  
number of different basis sets).

NSOP = number of symmetry elements generating the  
molecular point group to be used.

SYM (type CHARACTER) defines the symmetry elements.

XLIM = threshold for the integral calculation.

IUNIT = 0 assumes geometry input in atomic units.

" = 1 " " " " Angstrom.

IPR = print parameter. IPR=0 gives a minimum of  
printout, IPR=3 gives maximum.

Group 3: To be repeated NTYP times.

Record 3.1: BAS,NON,Q,SPDF,(JCO(J),J=1,5)

BAS (type CHARACTER) = identifier of a standard basis set to be read from a library (this will need some local modifications to work).

If BAS = 'blank' the basis set is read from the input file.

NON = number of symmetry-independent atoms using this basis set.

Q = nuclear charge.

SPDF (type CHARACTER) defines the highest L-value in this basis set.

JCO = number of groups of primitive GTOs for each L-value.

Note: Primitive GTOs in the same contraction are always in the same group. For efficiency reasons, one may also group together primitives that are not to be contracted. The performance of the code is related to the degree of grouping. Single GTOs should be avoided whenever possible.

Record 3.2: To be repeated NON times.

NAME, X, Y, Z

NAME (type CHARACTER) = label for each symmetry-independent atom.

X, Y, Z = Cartesian coordinates for each symmetry-independent atom.

Group 3.3: To be repeated for each L-value.  
(Group 3.3 is to be specified only if BAS = 'blank' in Record 3.1).

Record 3.3.1: (NUC(K), K=1, JCO(J))

NUC(K) = number of primitive GTOs in group K.

Record 3.3.2: (NRC(K), K=1, JCO(J))

NRC(K) = number of contracted functions (CGTOs) in group K.

Group 3.3.3: To be repeated JCO(J) times.

Record 3.3.3.1: (ALPHA(N), N=1,NUC(K))  
orbital exponents for the contraction group K.

Record 3.3.3.2: To be repeated NRC(K) times.

(CONT(N), N=1,NUC(K))  
contraction coefficients for the group K.